# AN EXPERIMENTAL INVESTIGATION OF THE BREAKUP OF A VISCOELASTIC NON-NEWTONIAN FLUID IN A SUPERSONIC STREAM

by

Kenneth Michael Chadwick

Thesis submitted to the Faculty of the

Virginia Polytechnic Institute and State University

in partial fulfillment of the requirements for the degree of

MASTER OF SCIENCE

in

Aerospace Engineering

APPROVED:

C. L. Yates, Chairman

J. A. Schetz

A. K. Jakubowski

October, 1990

Blacksburg, Virginia

# AN EXPERIMENTAL INVESTIGATION OF THE BREAKUP OF A VISCOELASTIC NON-NEWTONIAN FLUID IN A SUPERSONIC STREAM

by

Kenneth Michael Chadwick

Committee Chairman: Charlie L. Yates

Aerospace Engineering

(ABSTRACT)

A basic experimental study of the aerodynamic breakup of a viscoelastic non-Newtonian liquid injected into a supersonic stream was conducted. All test runs were made either at a free stream Mach number of 2.4 and a total pressure of 4.1 atm or a Mach number of 4.0 and a total pressure of 10.9 atm. The air flow had a total temperature of 300 K, and the injectant was always at room temperature. The injectant used for the majority of the test runs was diethylmalonate thickened with polymethyl-methacrylate, which has the characteristics of being viscoelastic. A limited number of test runs were made with glycerin in order to make a comparison between the behavior of Newtonian and viscoelastic non-Newtonian fluids. Several areas concerning the disintegration of the viscoelastic non-Newtonian fluid were investigated, including the effects of free stream Mach number, injection velocity, jet diameter, twin in-line jets, injection angle, and injector shape. Spark Shadowgraphs of 1.2 microsecond duration and high speed movies were obtained to qualitatively appraise the breakup behavior.

The breakup of the jet was found to be a function of free stream Mach number and jet diameter, injection angle, and frontal area. It also was observed that the breakup behavior of the viscoelastic non-Newtonian fluid is remarkably different from that of (Newtonian) glycerin. The time scales for breakup are substantially increased regarding the dissemination of the viscoelastic liquid as compared to the Newtonian glycerin. Furthermore, penetration of the viscoelastic non-Newtonian fluid was observed to be on the order of 50% less than that measured for glycerin at comparable injection conditions.

## ACKNOWLEDGEMENTS

As is usually the case, this work could not have been completed without the aid and support of others. I would first like to express my deepest gratitude to my wife for her love, support, and patience throughout the conduct of this study.

I also, wish to express my thanks to the members of my committee, Dr. Charlie Yates, Dr. Joesph Schetz, and Dr. Antoni Jakubowski, for their assistance and advice.

Among the many others who helped my efforts were Rodney Bowersox, Eric Fuller, Richard Mays, Maj. Charles Wood, Fei Kwok, Gary Stafford, Jake Frazier, Frank Shelor, and Kent Morris.

This work was supported by Teledyne Brown Engineering of Huntsville, Alabama with Martin Richardson as technical monitor.

## TABLE OF CONTENTS

## LIST OF SYMBOLS

$\alpha_j$ – injection angle relative to free stream

$d_j$ – injector diameter

$\gamma$ – ratio of specific heats

$\bar{h}$ – normalized penetration distance

$\Delta\bar{h}$ – normalized penetration of the actual value less the predicted value

$\bar{h}_{act}$ – actual jet penetration value

$M_\infty$ – Mach number of free stream

$P_\infty$ – static pressure of free stream

$P_{t,\infty}$ – total pressure of free stream

$\bar{q}$ – ratio of injectant-to-free stream dynamic pressures

$R$ – gas constant of free stream

$\rho_j$ – density of polymer solution

$\rho_\infty$ – density of free stream

$T_j$ – temperature of injectant

$T_\infty$ – static temperature of wind tunnel flow

$T_{t,\infty}$ – total temperature of wind tunnel flow

$v_j$ – velocity of injection

$v_\infty$ – velocity of free stream

$\bar{x}_h$ – normalized downstream distance

## LIST OF FIGURES

# 1.0 INTRODUCTION

## 1.1 Background

### *1.1.1 General*

The aerodynamic mechanisms by which liquid jets break up in a high speed crossflow are desirable to understand for many applications, including paint spraying, aerial dissemination of insecticides and fire retardants, explosive dissemination of fuel, and fuel atomization for liquid rockets and ramjets. However, these processes are complex. Many studies have been conducted and a considerable amount of literature is available for the breakup of Newtonian fluids in both subsonic and supersonic gas streams. For some applications, however, it is necessary to understand the process by which a highly viscous non-Newtonian fluid jet breaks up in an airstream. Low concentration polymer solutions have the characteristics of being both non-Newtonian and highly viscous. Currently, relatively little is known about the dissemination of these types of highly elastic fluids. Accordingly, the process by which these solutions breakup in both supersonic and subsonic streams has recently become of interest.

### *1.1.2 Newtonian Liquid Dissemination*

Many investigators have studied the dissemination of Newtonian liquid jets. Breakup of these jets is associated with the occurrence of instabilities in the jet. In turn, these instabilities are usually associated with an aerodynamic drag force

and the fact that the liquid-gas interface involves dissimilar physical properties and relative velocities. For the case of transverse injection these instabilities lead to the formation of aerodynamically induced waves on the windward side of the jet which are primarily responsible for the breakup.

The flow field of a liquid jet injected into a supersonic crossflow is two-phase, unsteady, turbulent, and three-dimensonal. Consequently, a theoretical analysis of the liquid jet breakup process is exceedingly complex. Typically, the cross-flow bends the liquid jet in the direction of the free stream flow. In addition, a boundary layer separation zone is produced just ahead of the jet near the injection point. This is caused by the interaction of the jet bow shock and the boundary layer on the surface of injection. These features of liquid injection are shown in Figure 1, which is a spark shadowgraph of a liquid injected transversely from a circular nozzle into a Mach 4.0 free stream.

Several investigators have studied liquid injection with limited success by employing analytical modeling techniques, including garden-hose and shedding-jet models.[1,2] These models have been primarily able to predict only jet penetration. By far, then, the majority of information on Newtonian jet dissemination has come from experimental investigations. Many aspects that affect the breakup have been studied experimentally, with most of the effort being related to the penetration, structure, atomization, and gross fracture of the jets.

The experimental investigations usually have involved either high speed movies (10,000 frames/s or greater) or very short exposure stills, or both. These have shown that the ultimate result of the jet breakup process is the formation of a cloud or spray of fine spherical droplets, and that jet penetration is a function of the square

root of a non-dimensional momentum flux parameter (See section 3.4). The effects of fluid properties on breakup, including viscosity and surface tension, have been studied by Nejad[3]. He found that by increasing liquid viscosity, penetration of the jet increased and formation of the droplet spray was retarded. The effect of surface tension was also studied. Its effect was that of enhancing droplet formation with a decrease in surface tension. The effect on penetration of varying the injection angle relative to the free stream flow has been extensively investigated and many empirical correlations have been developed. In the study by Baranovsky and Schetz[4], it was discovered that by increasing the angle of injecton relative to the free stream direction jet penetration reached a maximum at an angle of 135°, or 45° upstream. Joshi and Schetz tested many different injector configurations and their effects on jet penetration and spread in the study of Reference 5. They found that a rectangular -shaped jet aligned across the free stream penetrated further into the cross-flow than a circular jet of equivalent cross-sectional area. Hewitt and Schetz[6] documented the effect on atomization of impinging jets. They discovered that impinging jets atomized the fluid more completely than a singular circular jet. Numerous other investigators have done studies in this area. The bibliography of Reference 3 has a useful listing of many of these investigations.

### *1.1.3 Non-Newtonian Liquid Dissemination*

A non-Newtonian fluid may be classified as one that does not obey Stoke's Law.[7] In general, the fluid viscosity is a function of the rate of shear. Non-Newtonian fluids may be catagorized as being either inelastic or elastic, with the former usually referred to as being viscoelastic. The study of Reference 8 gives

a good account of the characteristic behavior of elastic fluid viscosity. Goldin, et. al.,[9] found marked differences between the breakup behavior of Newtonian, non-Newtonian inelastic, and viscoelastic jets. They observed that inelastic non-Newtonian jets behaved similarly to the Newtonian ones, but that the viscoelastic jets broke up into a series of thin threads or ligaments connecting non-spherical droplets.

The addition of small amounts of a polymer to a liquid can alter the process by which it disseminates tremendously. This phenomenon may be desirable for applications such as the antimisting of fuels in a post-crash aircraft situation, and the prevention of overly atomized forest-fire-fighting chemical agents.

Hoyt, et. al.[10] found that spray droplet formation is retarded by low concentration polymer solutions and that by increasing the polymer concentration the jet breakup is accompanied by ligaments connecting the droplets. Matta and Tytus [11] did an investigation of droplet size for the case of viscoelastic fluids injected into a 200 meter per second air stream. They found that the mass-median diameter for a viscoelastic fluid droplet is an order of magnitude larger than that of a comparable Newtonian fluid. They also suggested an elongational breakup mechanism. Andersen, et. al.[12] developed analytical models for a viscoelastic fluid in order to predict droplet size distribution and the length and width of the particle cloud for a wide range of subsonic air speeds. They suggest that surface stripping is the predominate breakup mechanism, and developed a model to predict its characteristics. They do, however, express a need for more experimental data, and consider detailed values of the droplet size and other characteristics predicted by their models to be approximate. Andersen and Polak [13] improved and extended the analytical

models from the just-mentioned study to include supersonic velocities. They found that droplet size increases with an increase in effective viscosity and a decrease in the fluid velocity. Also, they established temperature to be an influence on droplet size. As would be expected, an increase in the fluid temperature decreases the fluid viscosity, thereby reducing the droplet size. Comparable results were obtained by Hernan, et. al. [14] who conducted a series of tests involving a co-axial liquid jet. The polymer jet was injected with a flow velocity different from that of the surrounding airflow for the purpose of providing in- flight relaxation of the polymer solution after its initial aerodynamic breakup. They found a significant increase in the polymer solution breakup length with an increase temperature ranging from 20°C to 70°C.

## 1.2 Scope of the Investigation

The purpose of this study was to qualitatively investigate the breakup process of diethylmalonate (DEM) thickened with polymethyl- methacrylate (PMMA) under varying injector geometries at a simulated altitude and velocities. Polymethylmethacrylate is an elastic polymer, therefore, the solution consisting of the diethylmalonate (solvent) and the PMMA (solute) is of the viscoelastic type.

First, an apparatus had to be designed and built to inject the thickened diethylmalonate into the test section of the Virginia Tech supersonic wind tunnel facility. Included in this design was the ability to inject DEM not only normal to the free stream flow but at any desired angle and velocity.

Second, a test program was designed in order to investigate the effects of the following variables on the breakup process:

1. injector size
2. injector shape
3. orientation of the line of injection with the free stream
4. Mach number
5. injection velocity

The characteristics of the liquid jet that were observed are:

1. structure of the disintegrating jet
2. droplet size distribution
3. mechanisms of jet breakup
4. jet penetration

## 1.3 Methods of Investigation

Spark shadowgraphs and high speed movies were utilized in the investigation of the jet, the main stream-jet interaction, as well as limited downstream behavior of the injectant. For the most part , only the macroscopic behavior of the injectant was observed.

# 2.0 EXPERIMENTAL FACILITIES AND APPARATUS

## 2.1 The Wind Tunnel

The tests were conducted in the Virginia Tech supersonic wind tunnel. It is a blow-down type facility which utilizes sixteen storage tanks having a holding capacity of 79 cubic meters. The storage tanks are charged by four water-cooled reciprocating compressors (Ingersoll Rand Model 90). The compressed air is dryed and filtered to insure a clean flow. The wind tunnel has a 23 by 23 centimeter cross-section in the test section and is capable of producing Mach numbers of 2.4, 3.0, and 4.0 by the use of interchangeable two-dimensional nozzle blocks. The settling chamber contains a perforated cone and several screens for flow dampening. A pressure probe and transducer and a thermocouple provide settling chamber property information.

The test section is equipped with a manually controlled model mount which provides the ability to vary model position in the vertical plane. Large doors containing Schlieren quality windows provide excellent model accessibility.

During the period of time between the conduct of the Mach 2.4 and the Mach 4.0 tests of this study a new air charging, storage, and filtering system was installed. The charging system consists of a four-stage reciprocating air compressor (Ingersoll-Rand, Type HHE) driven by a 480 volt, 500 horsepower electric motor (Marathon Electric Company). The compressor can charge the two tank, 23 cubic meter storage system to 51 atmospheres.

The tunnel operating and control system includes a fast actuating butterfly valve and a 30.5-centimeter-diameter hydraulically actuated servo-valve for the purpose of pressure regulation. The wind tunnel total pressure is maintained constant for the duration of a test by the servo-valve, which incorporates a feedback loop utilizing pressure information from the settling chamber pressure probe.

## 2.2 The Liquid Injection System

### *2.2.1 The Flat Plate Model*

For the Mach 2.4 tests the thickened DEM was injected into the air stream from a stainless steel flat plate, with dimensions of 10.2 centimeters wide by 12.7 centimeters long and 0.8 centimeters thick. A series of interchangeable brass nozzles were used as injectors and these were located 5.1 centimeters from the sharp leading edge of the flat plate. Figure 2 illustrates the details of the flat plate and a typical injector.

A 2.0-millimeter-diameter circular nozzle configured for transverse injection was chosen as the baseline geometry. Four injectors were employed to yield jets angled with respect to the free stream from 45 degrees upstream to 45 degrees downstream (Figure 2 provides a description of the coordinate system). An additional five transverse injectors were constructed and their cross sections included 3.5 and 5.0 millimeter-diameter circles, a rectangular with a 2 to 1 aspect ratio and the equivalent area of a 2.0-millimeter-diameter circle, and two injectors whose initial 4.8-millimeter-circular cross sections were roughened with V-grooves in the axial direction to a depth of 10% and 20% of the initial diameter. The cross-sectional area of these last injectors were equivalent to that of a 5.0-millimeter-diameter circle.

The flat plate was mounted to a 33-centimeter long, 3.8-centimeter-diameter stainless steel sting. The plate-sting apparatus was then mounted in the wind tunnel test section to a model support mechanism which allowed for vertical plane positioning. The injectors were fed by a plenum chamber located on the underside of the flat plate and from which 0.95-centimeter-diameter copper tubing extended out of the wind tunnel and to the injection cylinder and accompanying hardware.

The plate-sting apparatus described above proved to be insufficient for the conduct of test runs at Mach 4.0. A redesigned brass flat plate was used with dimensions of 30.5 centimeters long by 15.3 centimeters wide and 0.8 centimeters thick. This plate was directly mounted to the wind tunnel test section floor with an aluminum wedge, which is 12.7 centimeters in height. (See Figure 3 for a complete description.) The injectors, as well as the hardware for feeding the liquid to them, remained as previously described.

### *2.2.2 The Injection Cylinder*

An air actuated, 170 atm piston-cylinder was used to force the thickened DEM to the flat plate model and then into the free stream. The piston-cylinder has an 20.3 centimeter stroke and a 6.4 centimeter diameter. Copper tubing with a 0.95 centimeter diameter and brass fittings were used to supply air for cylinder actuation.

Air for actuating the cylinder was provided by a bank of 150 atm breathing air tanks by way of a high pressure regulator which was used to control injectant flow rate by maintaining a predetermined pressure. Actual initialization of the injectant flow was achieved with a shop-air-actuated, quarter turn, 205 atm ball valve. Control of the shop air was provided by a computer-controlled electric solenoid together with a DC to AC relay.

Loading the DEM into the cylinder was accomplished by back filling from a tank containing the fluid. A ball valve was used to select the routing either to the tank or to the flat plate model. During the filling mode the piston was extracted and the cylinder was easily charged. See Figure 4 for a sketch of the entire system.

# 3.0 INSTRUMENTATION AND PROCEDURES

## 3.1 Instrumentation

The total pressure in the settling chamber was measured with a Pitot probe and a 0-100 psi 50 millivolt per psi pressure transducer (Setra Systems). The total pressure signal is also used in the wind tunnel control feedback circuit to regulate the wind tunnel total pressure.

The total temperature in the settling chamber was measured with a precision wire butt-welded chromel-alumel thermocouple (Omega Engineering Inc.). The signal was amplified by a thermocouple DC millivolt amplifier (Omega Inc., Model Omni IIB,Type K) and a differential DC amplifier (Ectron, Model 562) to give a total gain of 1000. The signal was then filtered with a 4 pole Bessel filter with a cut-off frequency of 340 Hz before being recorded.

## 3.2 Data Acquisition

Tunnel operation and data acquisition was controlled by an IBM-PC. The computer contains a multifunction, high speed, A/D I/O expansion board (Metrabyte Corp., Model DAS-16F) with a maximum sampling rate of 100 Khz. The computer monitored tunnel operation, sampled the various instrumentation functions, and sent remote signals to operate the fluid injection hardware and to control the acquisition of data. Figure 5 shows a schematic of the instrumentation system. The PC has 512k RAM and clock speed of 4.7 Mhz.

## 3.3 Flow Rate Measurement

A magnetic reed switch with an actuation time of less than a millisecond, along with a high speed waveform recorder was used to obtain information about the thickened DEM injection velocity.

A magnetic actuator was fastened to the piston stem of the injection cylinder. The magnetic reed switch was placed in close proximity to the piston stem so that the switch would close for a time corresponding to 2.5 centimeters of piston stem travel as the magnetic actuator passed by during injection. A direct current power supply was connected to the terminals of the reed switch so that when the switch was in the closed position a 5 volt signal was obtained. For the Mach 2.4 test runs a waveform recorder (LeCroy Model 6810) with a 5 Mhz maximum sampling rate was used to monitor and record the information from the reed switch during injection. LeCroy CATALYST software was used to control the data acquisition.

The 2.5 centimeters of piston stem travel which occurred while the reed switch was closed was related to the volume of injected fluid from a knowledge of the cylinder diameter. By analyzing the data recorded by the waveform recorder the total time required to inject the known volume of DEM was obtained. The injection velocity was then computed from the inferred flow rate and the known cross-sectional area of the injector.

For the Mach 4.0 test runs an improved technique was employed to monitor the information from the reed switch. The previously described A/D I/O expansion board (see section 3.2) was used to sample the signal from the reed switch at 10 Khz. This information was stored on floppy disk and was used in the program described in Section 3.6.

## 3.4 Photography

The camera and lens arrangement is schematically shown in Figure 6. Spark shadowgraphs were used throughout for the still photographic results. The shadowgraphs were backlighted photographs of short duration exposure.

The light source used was a strobe light (General Radio Company, Type 1531-AB Strobotac) having a 1.2 microsecond flash. The light intensity was set on the lowest position. The light source was placed at the focus of a 30.5 centimeter parabolic mirror (1.8 meter focal length), which was used to pass a parallel beam of light through the test section of the wind tunnel. Another 30.5 centimeter parabolic mirror was used to converge the image to a focal point where a lens with a 1.0 meter focal length was placed. The image was then focused on the view plane of a view camera (Burke and James Co.) with a 10.2 by 12.7 centimeter film holder (Polaroid , Model 545). To record a photograph, the laboratory lights were darkened and the source was remotely operated by the computer control to expose the film. Polaroid Type 57 (ASA 3000) film was used throughout. A 0.635 centimeter square grid was provided in the background of the photographs to facilitate the resolution of the jet dimensions.

Several high speed movies were taken with either a full frame movie camera (Wollensak- Fastax Model J-515) having up to 6000 frames per second operating speed or a quarter frame camera (Hycam) having up to 36000 pictures per second operating speed. The movies were backlighted with a 1000 watt incandesant light source, as well as ambient laboratory lighting (see Figure 7). Kodak Type 7277, 4-x reversal, 16 millimeter film in rolls (30.5 meter) was used throughout.

## 3.5 Experimental Procedure

All tests completed for this study were run at Mach number equal to 2.4 or 4.0. A total pressure of 4.1 $\pm$.2 atm was maintained for all tests at Mach 2.4, and 10.9 $\pm$.3 for those at Mach 4.0. The total temperature in the wind tunnel was nominally 300 K, and the temperature of the DEM was that of the laboratory, approximately 25°C.

A typical test run was completed in the following manner. The wind tunnel was started, and after a few seconds to allow total pressure oscillations to dampen out, the PC initiated the injection of the DEM and the acquisition of the flow rate data. At the instant the magnetic reed switch of the flow rate measurement system closed, the PC actuated the flash of the strobe light. The tunnel was then allowed to run a few seconds longer to clean out any spurious accumulation of DEM in the test section.

A run that involved a high speed movie was accomplished in a similar manner, except that the movie camera was started by the PC at the instance of injection, and the light source remained continually in operation until it was manually deactivated.

The flow rate data was evaluated on-line and made available for on- screen observation, as well as in hardcopy form by an accompanying printer. A computer program, INJECT.BAS, was written and used to control the tunnel operation and injection process. The listing of this program is in the appendix.

The injectant used for all the tests was a polymer solution whose constituents were diethylmalonate thickened with 5% polymethyl methacrylate and included a trace of calico blue dye. This solution has a density of 1045 $kg/m^3$ and a viscosity of 298 centipoise at a shear value of 12.6$s^{-1}$.

## 3.6 Determination of the Momentum Flux Parameter

It is customary in the study of fluid injection into supersonic streams to correlate results in terms of a non-dimensional momemtum flux parameter. This parameter, whose value was prescribed for each test run, is also the ratio of the dynamic pressure of the injectant to the dynamic pressure of the free stream and can be expressed in equation form as:

$$\bar{q} = \frac{\rho_j \, {v_j}^2}{\rho_\infty \, {v_\infty}^2}$$

The above expression is calculated in the following manner, assuming calorically perfect isentropic flow:

$$P_\infty = P_{t,1} \left(1 + \frac{\gamma - 1}{2} M_\infty^2\right)^{-\gamma/(\gamma-1)}$$

with,

$$\rho_\infty = \frac{P_\infty}{R \, T_\infty}$$

and with,

$$v_\infty^2 = M_\infty^2 \, \gamma \, R \, T_\infty$$

It can be easily derived by substitution for $\rho_\infty$ and ${v_\infty}^2$ that

$$(\rho \, v^2)_\infty = \gamma \, M_\infty^2 \, P_{t,1} \left(1 + \frac{\gamma - 1}{2} M_\infty^2\right)^{-\gamma/(\gamma-1)}$$

The unknown parameter in the denominator of the $\bar{q}$ equation is the $v_j$ term. This term can be expressed as:

$$v_j = \frac{\text{volume of the injected fluid}}{(\text{duration of injection})\ (\text{cross} - \text{sectional area of the injector})}$$

The value of the duration-term in the above expression is the measured time determined by the method described in Section 3.3. The other terms in the above express are chosen parameters. A BASIC program was written to calculate $\bar{q}$ from the information stored on floppy disk, which was described in Section 3.3. This program, QBAR.BAS, is listed in the appendix.

# 4.0 RESULTS AND DISCUSSION

A transversely-directed, circular orifice of diameter $d_j = 2.0$ mm was chosen as the base injector geometry for this investigation. For this base geometry, the effects on jet breakup of varying the fluid type, $\bar{q}$, and Mach number are discussed in Section 4.1.1. In the subsequent subsections, the effects of jet diameter, in-line jets, injection angle, and injector shape are discussed, again in terms of jet breakup. In the final subsection, the results related to jet penetration are discussed. In viewing the following data, it should be recalled that there is a 0.635-centimeter-square grid in the background of all the photographs.

## 4.1 Jet Breakup

### 4.1.1 Fixed-Diameter Circular Orifice

The parametric variations made with the $d_j = 2.0$ mm circular orifice consisted of fluid type, magnitude of the dynamic pressure ratio, $\bar{q}$, and Mach number of the airflow.

#### *4.1.1.1 Effect of Fluid Type at Mach 4.0*

In order to provide a basis for comparing the behavior of the viscoelastic and Newtonian fluids, some test runs were made at Mach 4.0 with glycerin as the injectant. The viscosity of the glycerin was 300 centipoise, which is also approximately the value for the DEM at a shear rate of 12.6 $s^{-1}$, as reported by the supplier

(Teledyne Brown Engineering). Presented in Figure 8 are four shadowgraphs, two for the DEM and two for the glycerin. The values of $\bar{q}$ are 7.2 and 10.0 for both the DEM (Runs 164 and 163,respestively) and glycerin (Runs 246 and 243, respectively). The farthest downstream distance covered by these photographs is x= 25 cm, or $x/d_j = 125$.

There are some resemblances and striking differences in the breakup of the Newtonian glycerin and the viscoelastic DEM over the distance covered by the photographs. The shedding of ligaments is apparent in the dissemination of both types of liquid, but the glycerin jets break down much more rapidly into fine droplets, which are too small to be resolved in the shadowgraphs, and appear as a grayish cloud. On the other hand, while there is some fragmentation of the DEM jets, there are very few discernible droplets present in the near field. Rather, the observed breakup of the DEM jets is characterized by the erratic stripping of threads or ligaments from the main jet body. There is evidence in Figure 8, at least for the higher $\bar{q}$, that the ligaments are undergoing a further breakup into smaller, highly asymmetric particles. (Additional evidence of this is presented in Section 4.1.1.2.) Since all flow conditions are essentially equivalent for the corresponding glycerin and DEM tests, it appears that the differences in the observed jet breakup can be attributed to the elasticity of the DEM.

#### *4.1.1.2 Effect of $\bar{q}$ at Mach 2.4 and 4.0*

All tests for a given Mach number were made with essentially constant wind tunnel dynamic pressure. Therefore, the variation produced in the dimensionless momentum flux parameter, $\bar{q}$, pertains only to a variation in the injection velocity

at a particular Mach number. As shown in Figures 9 and 10 for Mach 2.4, an increase in the value of $\bar{q}$ from 6.5 to 15 for a fixed injector geometry tends to decrease the length required for major fragmentation of the jet. At the highest $\bar{q}$ of 15, a significant number of relatively small particles of liquid are present by $x/d_j = 125$, which is the farthest downstream distance covered in these photographs. This general dependency of breakup length on $\bar{q}$ is also observed for jets of differing sizes and geometries.

Based on the present results, however, there are two reasons why it is not possible to obtain even a rough estimate of the quantitative dependency of the fracture length on $\bar{q}$. In this connection, it is important to note that Figures 9 and 10 are two realizations of results obtained for duplicated test conditions. The first impediment to a quantitative analysis lies in the fact that it is difficult to provide an exact definition of the fracture length itself, given the complex geometry of the disintegrating jet as seen in either Figure 9 or 10. The second impediment is related to the inherent unsteadiness of the interaction between the jet and the airstream which can be seen by comparing corresponding photographs (same $\bar{q}$) between Figures 9 and 10. Especially at the lowest value of $\bar{q} = 6.5$, a significant difference in the apparent fracture length is observed between Figures 9 and 10.

The observed unsteadiness is shown even more dramatically by high speed movies of the injection process. This, in fact, was the main piece of information gained from the small number of such movies taken in this investigation. Figure 28 presents 5 consecutive frames (top to bottom) of a high speed movie taken in this study. The test conditions are that of the baseline injector (2.0-mm-diameter circle) at Mach 2.4 and with $\bar{q} = 20$. The film speed is approximately 2000 pictures

per second. This speed results in an exposure time that is about 400 times longer than that obtained for the still photographs. In view of the unsteadiness that is nevertheless observable in this figure, it is clear that a larger number of samples of still photographs would be required for the purpose of estimating a mean value of the fracture length, assuming that such a length could be defined.

The results obtained for the effect of $\bar{q}$ at Mach 4.0 are shown for a single realization in Figure 11, which also covers a downstream distance of $x/d_j = 125$. A somewhat greater range of $\bar{q}$ was obtained for these tests, varying between 7.2 and 22.0. Regarding the effect of $\bar{q}$ on the fracture length, and the general complexity and unsteadiness (to be shown in Figure 12) of the breakup process, the behavior at Mach 4.0 is very similar to that observed at Mach 2.4. There does appear to be, however, a stronger tendency for the jet to bifurcate at the higher values of $\bar{q}$ ($\bar{q} >$ 15).

#### *4.1.1.3 Effect of Mach Number*

Figure 12 contains two sets of photographs, one set consisting of two realizations at Mach 2.4, and one set for two realizations at Mach 4.0. All four test runs have $\bar{q}$ equal to 15. From these figures it is clear that the jets of the two test runs at Mach 2.4 breakup earlier and penetrate further into the crossflow than those at Mach 4.0. It should be noted, though, that the dynamic pressures of both the free stream and the jet differ between the two Mach numbers. Therefore, it must be accepted that only the ratios of the dynamic pressures, $\bar{q}$, is relevant if the differences seen in Figure 12 are to be associated with a pure Mach number effect.

### 4.1.2 Effect of Injector Diameter on Jet Dissemination

Figures 13 and 14 illustrate two realizations of results from a series of test runs at Mach 2.4 with the injection velocity held constant, $\bar{q} = 15$, and the diameter of the circular injectors varied from 2.0 to 5.0 millimeters. Figure 15 shows a singular realization of the results obtained for the same conditions, but at Mach 4.0.

It appears from the results at Mach 2.4 that the mean length of major jet fracture is not discernibly dependent on injector diameter. On the other hand, the size of the initial fragments do scale with the diameter. Therefore, the downstream distance required to obtain a given particle mean size increases with jet size. For Mach 4.0, however, it seems clear that a decrease in the jet diameter leads to a significantly reduced fracture length, along with the subsequently smaller particle sizes. Moreover, as a first approximation, it would appear that fracture length at Mach 4.0 scales directly with jet diameter. The inability to make the same kind of definitive statement for the Mach 2.4 results is due to the higher degree of breakup activity at the lower Mach number which tends to obscure the point of jet fracture.

### 4.1.3 Effect of Twin In-Line Jets

In Reference 16 it is shown for Newtonian liquids that when one jet shields another from the airflow the shielded jet penetrates roughly twice as far into the free stream. Figure 16 illustrates three realizations at $\bar{q} = 15$ of the interactive behavior of twin in-line jets of DEM found in this study at Mach 2.4. The diameter of each jet was 2.0 mm and they were spaced apart by 5.0 mm. Figure 17 shows singular realizations obtained with the same injector for values of $\bar{q}$ between 12 and 25.5 at

Mach 4.0. It is clear for either Mach number that the second jet penetrates more than the shielding jet, but certainly does not show nearly the increased penetration observed for Newtonian jets in Reference 15. Rather, the two jets rapidly merge to form a single jet, and it appears that dissemination is significantly retarded, even to the extent that breakup is slower than that observed for a single jet of either the same diameter or of the equivalent total cross-sectional area.

In support of this observation, it is first noted for Mach 2.4 and $\bar{q} = 15$ that certainly the jet breakup and perhaps even the penetration is less for the two, 2.0 mm jets of any of the realizations shown in Figure 16 than was observed for a single, 2.0-mm jet and the same $\bar{q}$ in either Figure 9 (first realization, Run 109) or Figure 10 (second realization, Run 110). Second, it is noted that although the total cross-sectional area of two, 2.0-mm-diameter jets falls between the area of single jets of 2.0 mm (50% less) and 3.25 mm (32% greater), the extent of the breakup observed in Figure 16 does not fall between that observed for Runs 109 and 131 in Figure 13, or Runs 110 and 133 in Figure 14. In fact, the breakup for the two-jet arrangement appears less advanced than that observed for the single, 5.0-mm-diameter jet shown in Figure 13 or 14. Moreover, the results obtained for the in-line jets are consistent with an observation that will be made later regarding a rectangular injector in Section 4.1.5, where it is noted that it is an increase in frontal area as opposed to the total cross-sectional area that promotes jet breakup.

Regarding the in-line injector results obtained at Mach 4.0, it is noted again that the extent of breakup for the same value of $\bar{q}$ ($\bar{q} = 15$) is significantly less for the in-line injector than for a single injector of the same diameter (compare Run 200 of Figure 17 with Run 159 of Figure 15), or for a single injector of the

same total cross-sectional area (compare Run 200 of Figure 17 to an interpolation of Runs 159 and 207 in Figure 15). Also, the data shown in Figure 17 suggests that this conclusion is valid for other values of $\bar{q}$, at least up to $\bar{q} = 25.5$. (Recall the bifurcation that was noted for a single, 2.0-mm-diameter jet at $\bar{q} = 22$ in Figure 11.)

### 4.1.4 Effect of Injection Angle

In the case of Newtonian fluid injection it has been found that jets inclined upstream to the flow penetrate farther into the free stream than jets inclined otherwise. Baranovsky and Schetz obtained typical results in the study of Reference 4. Similar results regarding penetration were also observed in the present study of viscoelastic liquid jets. Namely, the jets that were directed upstream consistently penetrated farther into the flow. More importantly, however, the present results clearly show that injection angle has a significant effect on major jet fragmentation.

#### *4.1.4.1 Results for Mach 2.4*

Figures 18 and 19 illustrate the results from a series of test runs at Mach 2.4 conducted with fixed injection velocity ($\bar{q} = 15$) and jet diameter (2.0 mm) while varying the angle of injection to the free stream (see Figure 2 for a description of the coordinate system used). In particular, the injection angle was varied from $45^o$ upstream ($\alpha_j = 45^o$) to $45^o$ downstream ($\alpha_j = 135^o$). The results show that jets inclined upstream experience earlier fragmentation of the main jet body and undergo earlier breakup into smaller particles than is observed for normal or downstream-angled jets. Consequently, as the angle of injection is increased from a downstream

to an upstream direction the distance required for jet dissemination is significantly reduced. It is anticipated, however, that in terms of promoting jet breakup there is probably an optimal, upstream injection angle. More extensive data beyond the present results would be needed to determine such an optimum.

*4.1.4.2 Results for Mach 4.0*

Figures 20 and 21 show the effect of $\bar{q}$ for upstream injection at Mach 4.0. The jets in Figure 20 are at 45°, and those in Figure 21 are at 60°. In each case the general trend appears to be that jet dissemination is enhanced by increased $\bar{q}$, which feature was previously noted in connection with normal injection (see Section 4.1.1.2). When results for the same values of $\bar{q}$ are compared between Figures 20 and 21 (Runs 183 and 167 for $\bar{q}$ = 19.3, and Runs 189 and 172 for $\bar{q}$ = 22), it is still not possible to state unequivocally which value of upstream angle, $\alpha_j$ = 45° or 60°, leads to the greatest degree of jet breakup, although it appears roughly that $\alpha_j$ = 45° is superior. Much of the ambiguity in this connection is due to the natural unsteadiness of the breakup process. What is clear from Figures 20 and 21, however, is that upstream injection at Mach 4.0, just as at Mach 2.4, leads to significantly enhanced jet breakup when compared with normal injection (see Figure 11).

Regarding the downstream injection at Mach 4.0, Figures 22 and 23 show the effect of $\bar{q}$ for the jets at $\alpha_j$ = 120° and $\alpha_j$ = 135°, respectively. For $\alpha_j$ = 120°, there appears to be a discernible effect of jet breakup being accelerated by increased $\bar{q}$. It is interesting, however, to compare in Figure 22 the results for Run 178 ($\bar{q}$ = 18.5) with those of Run 180 ($\bar{q}$ = 25.5), which suggests that jet breakup is more pronounced at the lower $\bar{q}$. It is believed that this comparison is a clear example of

how the unsteadiness of the jet breakup process can lead to erroneous conclusions when a limited number of data samples are available.

For the case of $\alpha_j = 135^o$, the level of jet breakup activity is so diminished for all values of $\bar{q}$ tested it is difficult to identify a noticeable effect of $\bar{q}$. Moreover, by comparing the results of both Figure 22 and 23 with those of Figure 11, it is again obvious, just as for Mach 2.4, that downstream injection is less effective than normal injection in terms of jet breakup.

Since the time scales for jet breakup under the conditions associated with the results for $\alpha_j = 135^o$ in Figure 23 are apparently longer than the times of observation covered by the photographs, the recorded jet motions provide some insight into the early stages of the breakup process. What is observed is that, in addition to wave-like disturbances that propagate along the jet axis, there is significant stretching and thinning of the jet body. It is believed that the ability of the jet to support such deformations is due at least partly to the elasticity of the test liquid.

### 4.1.5 Effect of Injector Shape

#### *4.1.5.1 Effect of Rectangular Shapes*

Some tests were run for the case of normal injection from a rectangular injector which had a 2-to-1 aspect ratio and an area equivalent to that of the 2.0-mm-diameter circular injector. Runs were made with this injector aligned with the flow and across the flow at Mach 2.4 and 4.0. Figure 24 illustrates typical results for $\bar{q} = 15$ at Mach 2.4, and Figure 25 does the same for $\bar{q} = 15$ at Mach 4.0. By comparing these limited results with those for the corresponding circular injector,

samples of which are included in Figures 24 and 25, it appears that slightly retarded fragmentation occurs in the case of the rectangular injector aligned with the flow. This conclusion holds true for test runs made at both Mach numbers. On the other hand, it is noticeable in Figures 24 and 25 that the initial fragmentation is augmented over what occurs for the circular jet when the rectangular injector is aligned across the flow. This suggests that the breakup of the jets may generally be enhanced by increasing the jet frontal area for a given cross-sectional area.

*4.1.5.2 Effect of Injector Roughness*

Figures 26 shows the results of tests run at Mach 2.4 for two values of $\bar{q}$ with the 10% roughened-circular injector described in Section 2.2.1. Included in this figure are results that were discussed earlier for the 5.0 mm, circular injector. Recall that this roughened injector was designed to have a cross-sectional area equivalent to that of the 5.0-mm-diameter circular injector, but with 10% roughness elements. By comparing the corresponding smooth and roughened circular results, it appears that the modest amount of roughness employed here does not significantly alter jet dissemination.

The preceding conclusion is further supported by the results of tests run at Mach 4.0 with a different, roughened-circular injector. The latter injector had roughness elements equal to 20% of its diameter, and an area equivalent to that of a 5.0-mm-diameter circle (see Section 2.2.1). Injection results were obtained for two values of $\bar{q}$, and they are shown along with some pertinent, smooth-circular results in Figure 27. Again, no noticeable difference in the jet breakup behavior is observed between the roughened and smooth injectors.

## 4.2 Penetration

### *4.2.1 Penetration of Normal DEM Jets*

Based on the unsteadiness and the diminished breakup observed for the viscoelastic over the Newtonian jets of this investigation, and given the necessity for a larger number of samples for any statistical representations, an attempt to formulate a penetration correlation does not seem feasible. Especially because of the short exposure time of the photographs, the observed instantaneous boundaries between the DEM jets and the free stream generally do not define a smooth, well delineated curve. Consequently, it is not possible to describe the maximum penetration boundary in terms of an analytical function. This situation is very much unlike that observed for Newtonian jets, e.g., the results shown for glycerin in Figure 8, which, apparently due to a higher frequency of the unsteadiness and a greater degree of breakup, display a well-defined upper jet boundary even for the same exposure time. Nevertheless, it is still of interest to point out some of the salient features of the jet penetration behavior observed in the present study for a viscoelastic fluid, and to compare this behavior with what has been previously documented for Newtonian fluids.

To begin with, it is noted that the results presented in Figure 8 make possible to compare the penetration behavior of DEM and glycerin jets for two values of $\bar{q}$ at Mach 4.0 (Runs 246 and 164 at $\bar{q} = 7.2$ and Runs 243 and 163 at $\bar{q} = 10$). The obvious difference is that the DEM jets penetrate much less into the cross flow than the glycerin jets. Moreover, from these photographs it appears that the DEM penetration is on the order of one-half the glycerin penetration.

Figures 9, 10, and 11 illustrate results obtained for the normal injection of DEM with increasing $\bar{q}$. Figures 9 and 10 are for Mach 2.4, and Figure 11 is for Mach 4.0. From these figures it is apparent that the overall trend is to increase penetration as $\bar{q}$ is increased. In the case of Newtonian fluid injection it is accepted that penetration is related to $\bar{q}^{0.5}$[4,15]. For the present results, however, this relationship does not appear to be valid. The basis for this conclusion becomes apparent by noticing in these figures that with a small increment in $\bar{q}$ penetration is not necessarily increased (see Figure 11, Runs 157 and 159 for example). It should be noted, though, that the unsteadiness of the breakup process makes it difficult to define precisely what the actual penetration is at a given downstream location. It may be necessary, therefore, to obtain photographic results with a longer exposure time before any definitive conclusions can be drawn.

### *4.2.2 Effect of Twin In-Line Jets*

In Reference 16 it is shown for Newtonian liquids that when one jet shields another from the airflow the shielded jet penetrates farther into the free stream. In fact, second jet was found to penetrate roughly twice as far as the shielding jet. Figure 17 illustrates three realizations of the interaction of twin, in-line, viscoelastic jets found in this study at Mach 2.4. Figure 18 shows comparable results obtained at Mach 4.0. It is clear from these photographs that the second jet penetrates only slightly more than the shielding jet, and certainly not near the penetration observed for the Newtonian jets of Reference 16.

### *4.2.3 Effect of Injector Shape*

In the study by Joshi and Schetz[5], it was observed that the penetration of Newtonian fluids was slightly greater for a rectangular jet aligned across the free stream than it was for a circular jet having an equivalent cross-sectional area. Figures 24 and 25 illustrate the relevant results found for DEM in this study at Mach 2.4 and Mach 4.0, respectively. By comparing these limited results with those obtained for the corresponding circular injection cases it appears that the penetration of neither the jets aligned with the flow nor across the flow is significantly increased over that for circular injectors. No noticeable difference in the penetration of the jets from the roughened injector over the smooth injector is not apparent.

### *4.2.4 Effect of Injection Angle*

As was stated in Section 4.1.4, it has been found that jets inclined upstream penetrate farther into the free stream than those inclined otherwise. It can be stated definitively from the results of this study that as the injection angle is increased from a downstream to an upstream direction penetration is increased at both Mach 2.4 and 4.0 (see Figures 18-23). In the case of Newtonian liquid jets (reference 4), maximum penetration was observed to be at or near $\alpha_j = 45^o$. In the present study, maximum penetration was observed to be also achieved by the upstream-directed jets, but given the extent of the jet breakup it cannot be stated that penetration at $\alpha_j = 45^o$ is greater than that at $\alpha_j = 60^o$.

# 5.0 CONCLUSIONS

The injection apparatus employed for these tests functioned well. Injection rates were easily established and the use of computerized test control, as well as the ease with which injectors could be interchanged allowed for the rapid conduct of numerous test runs without difficulty. Also, the employed photographic techniques successfully illustrated some major features of the liquid jet-free stream interaction.

Several significant results were observed: First, breakup of the DEM jets occurs when ligaments are stripped from the surface of the main jet body. These ligaments are consequently broken into smaller ligaments. Some of the smaller ligaments fracture to form asymmetric particles. The fluid elasticity was observed to significantly retard the jet dissemination process. Second, increasing the injection velocity decreased the downstream distance required for major fragmentation of the jet. An analytical relationship between the fracture length and the injection velocity of the jet was not obtainable for two reasons. It is difficult to define the fracture length because of the nebulous character of the breakup pattern. Also, an unsteadiness of the entire breakup process would require many more samples of data than what was obtained before any statistical representation would be valid. The factor which had the most profound effect on the breakup process was the angle of injection with respect to the free stream. As the angle of injection was increased from a downstream direction to the upstream direction the distance required for jet dissemination was significantly reduced. Also, an increase in Mach number from 2.4 to 4.0 reduced the dissemination of the liquid DEM as well as decreasing the

penetration of the jet into the crossflow. It was observed that an increase in frontal area enhances the jet breakup, as in the cases of rectangular jets aligned at different aspects to the airflow. The effect of injector roughness was not observed to have any effect on jet dissemination in this study. In the case of twin jets the downstream jet did not penetrate as far into the flow as that which is normally observed with Newtonian fluids, and jet breakup was observed to be less than that of a single jet of equivalent cross-sectional area. The normally-directed elastic jets penetrated the crossflow on the order of 50% less than that observed for a Newtonian jet (glycerin) having an equivalent set of flow conditions. Injection angle also has a large effect on the penetration of elastic jets. The upstream- directed jets consistently penetrated the cross flow more than those directed otherwise. Development of a penetration correlation for the DEM jets was not possible in this study given the number of samples available and the inherent unsteadiness of the breakup process.

# BIBLIOGRAPHY


1. Forde, J. M., Molder S., and Szpiro, E. J., "Secondary Liquid Injection into a Supersonic Airstream", J. of Spacecraft and Rockets Vol. 3, 1172-1176.
2. Adelberg, M., "Breakup Rate and Penetration of a Liquid Jet in a Gas Stream", AIAA Journal, Vol. 5, No. 8, 1408-1415.
3. Nejad, A. S., "Effect of Physical Properties on Breakup and Atomization of Liquid Jets in a Supersonic Crossflow", Ph. D. Dissertation, Virginia Polytechnic Institute and State University, 1982.
4. Baranovsky, S. I. and Schetz J. A., "Effect of Angle on Liquid Injection into a Supersonic Flow", AIAA Journal, Vol. 18, June 1980, 625-629.
5. Joshi, P. and Schetz, J. A., "Effect of Injector Shape on Penetration and Spread of the Liquids", AIAA Journal, Vol. 13, Sept. 1975, 1137-1138.
6. Hewitt, P. W. and Schetz, J. A., "Effects of Injector Geometry on the Structure of a Liquid Jet Injected Normal to a Supersonic Airstream", AIAA Journal, Vol. 21, July 1983, 956-961.
7. Schetz, J. A., "Foundations of Boundary Layer Theory for Momentum, Heat, and Mass Transfer", Prentice-Hall Inc.; New Jersey, 1984.
8. Peng, S. T. J. and Landel, R. F., "Preliminary Investigation of Elongational Flow of Dilute Polymer Solutions", Journal of Applied Physics, Vol. 47, No. 10, October 1976, 4255-4260.
9. Goldin, M., Yerushalmi J., Pfeffer, R., and Shinnar, R., "Breakup of a Laminar Capillary Jet of a Viscoelastic Fluid", Journal of Fluid Mechanics, Vol. 39., 44-71.

10. Hoyt, J. W., Taylor, J. J., and Runge, C. D., Journal of Fluid Mechanics, Vol. 63, 1974, 635-640.

11. Matta, J. E. and Tytus, R. P., Journal of Applied Polymer Science, Vol. 27, 1982, 397-402.

12. Andersen, W. H., Louie, N. A., and Ialongo G., "Aerodynamic Breakup of Viscoelastic Liquids. Phase I. Subsonic Dissemination", Report 3400-12 (Final) to Edgewood Arsenal, Shock Hydrodynamics, October 1976.

13. Andersen, W. H., Polak, L. F., "Investigation of the Aerodynamic Breakup of Viscoelastic Liquids. Phase II Supersonic Dissemination", Report 3400-24 (Final) to Chemical Systems Laboratory, Shock Hydrodynamics, May 1978.

14. Hernan, M. A., Parikh, P., Yavrouian, A., and Sarhoia, V., "Aerodynamic Breakup of Polymer Solutions via Digital Image Processing Techniques", Report to Aberdeen Proving Ground, Jet Propulsion Laboratory, April 1986.

15. Yates, C. L., "Liquid Injection into a Supersonic Stream", AFAPL-TR-71-97, Vol. 1, 1972.

16. Hinson, W. F., Gooderum, P. B., and Bushnell, D. A., "Experimental Investigation of Multiple-Jet Liquid Injection into Hypersonic Flow", NASA TN D-5861, Langley Research Center, June 1970.

# FIGURES

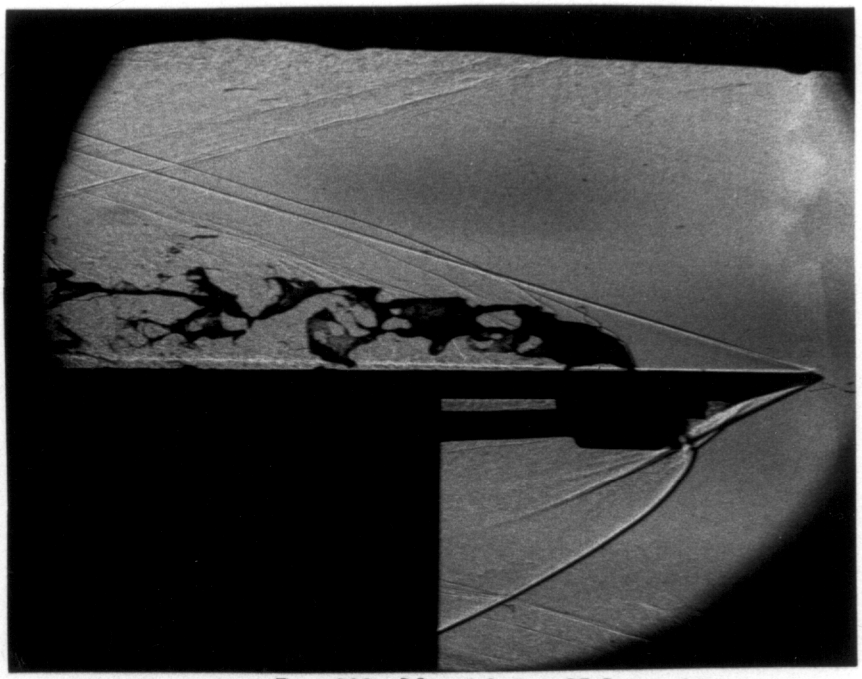

Run 233 : $M = 4.0, \bar{q} = 25.5$
injector type : circular, $d_j = 2$ mm, $\alpha_j = 90°$

Figure 1: Liquid Injection into a Supersonic Stream

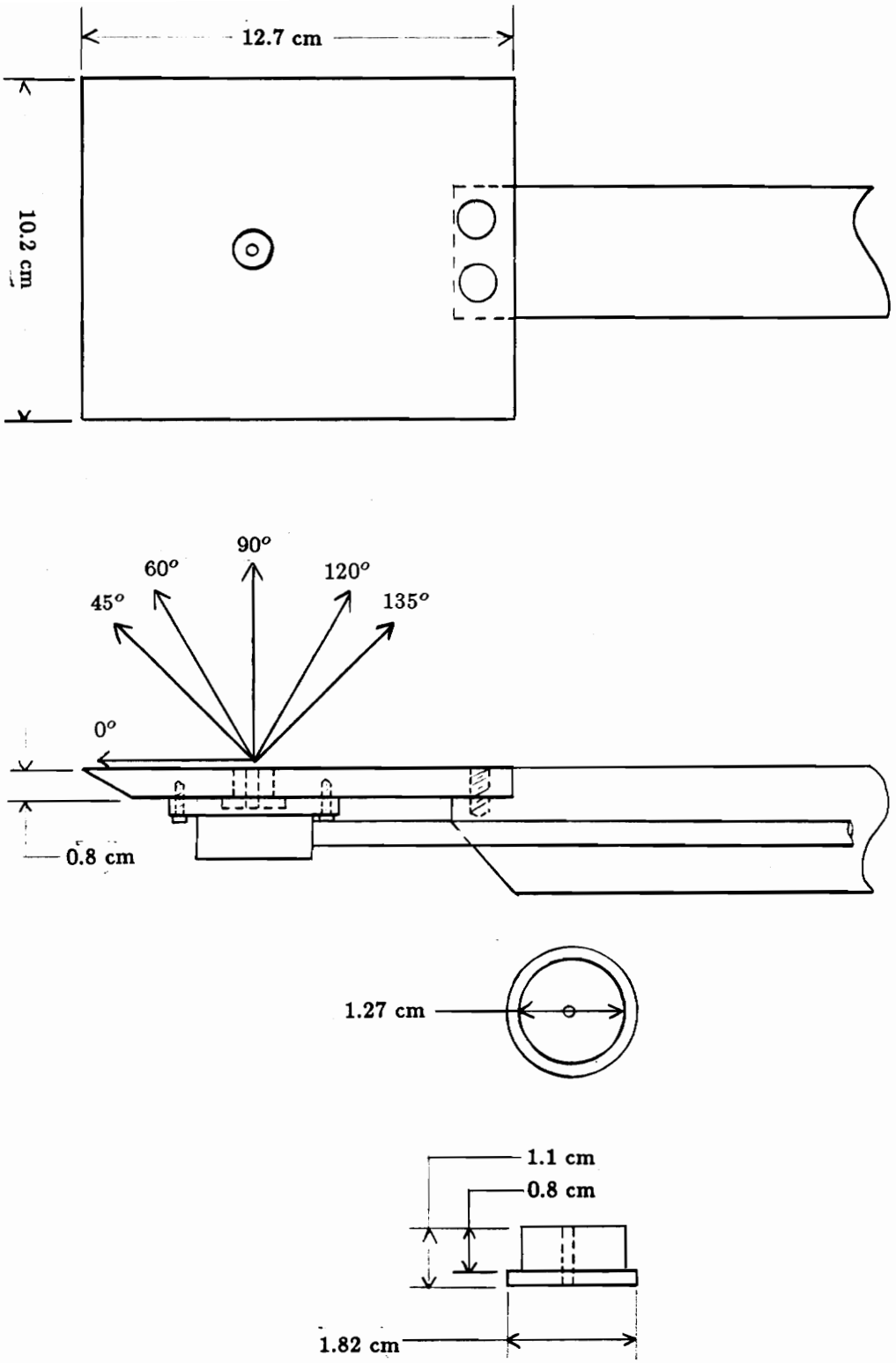


Figure 2: Sketch of the Flat Plate Model used for Mach 2.4

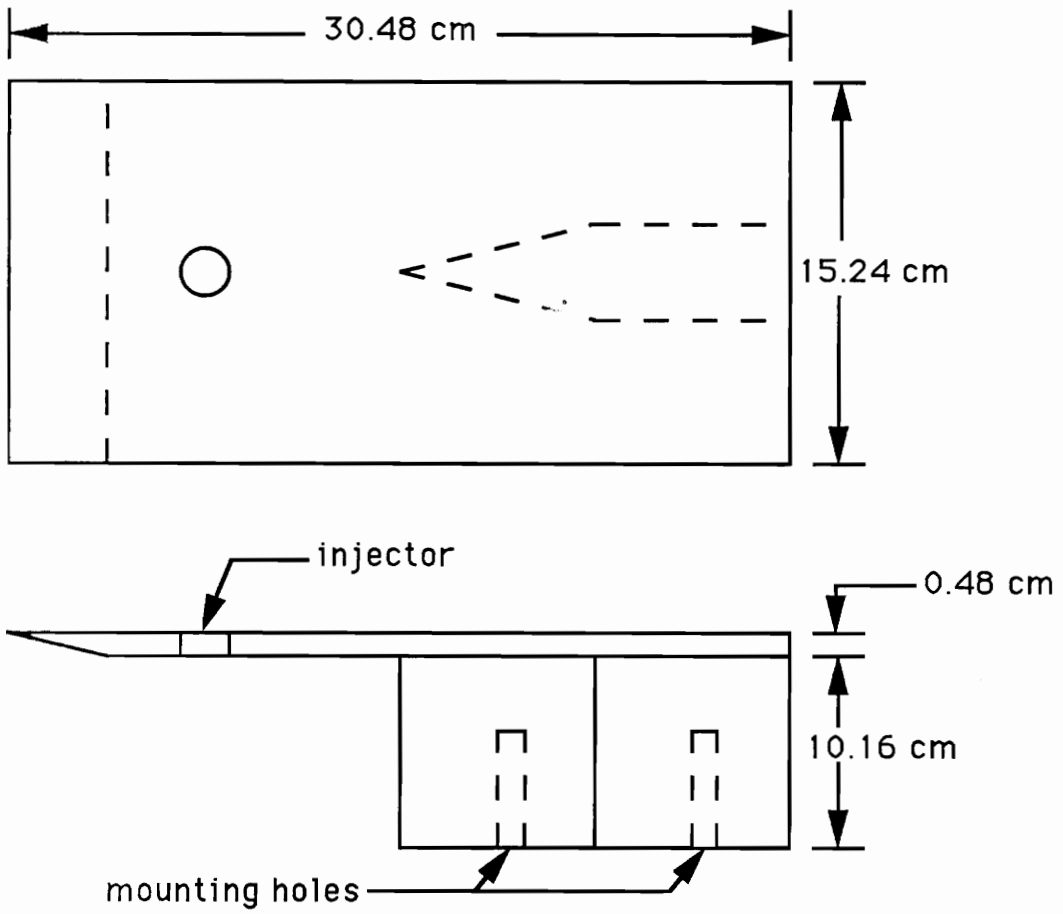


Figure 3: Sketch of the Flat Plate Model used for Mach 4.0

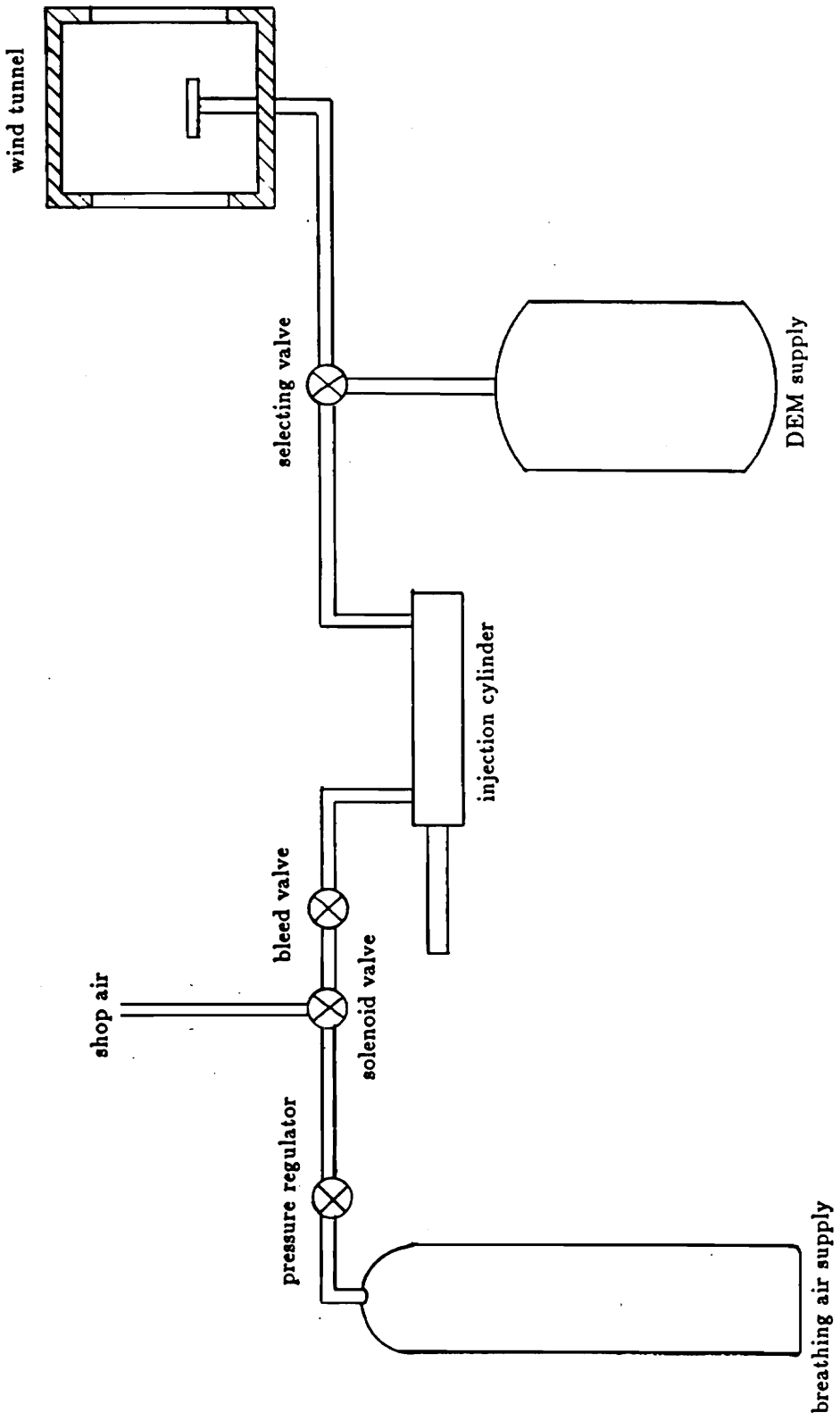


Figure 4: Schematic of the Injection System

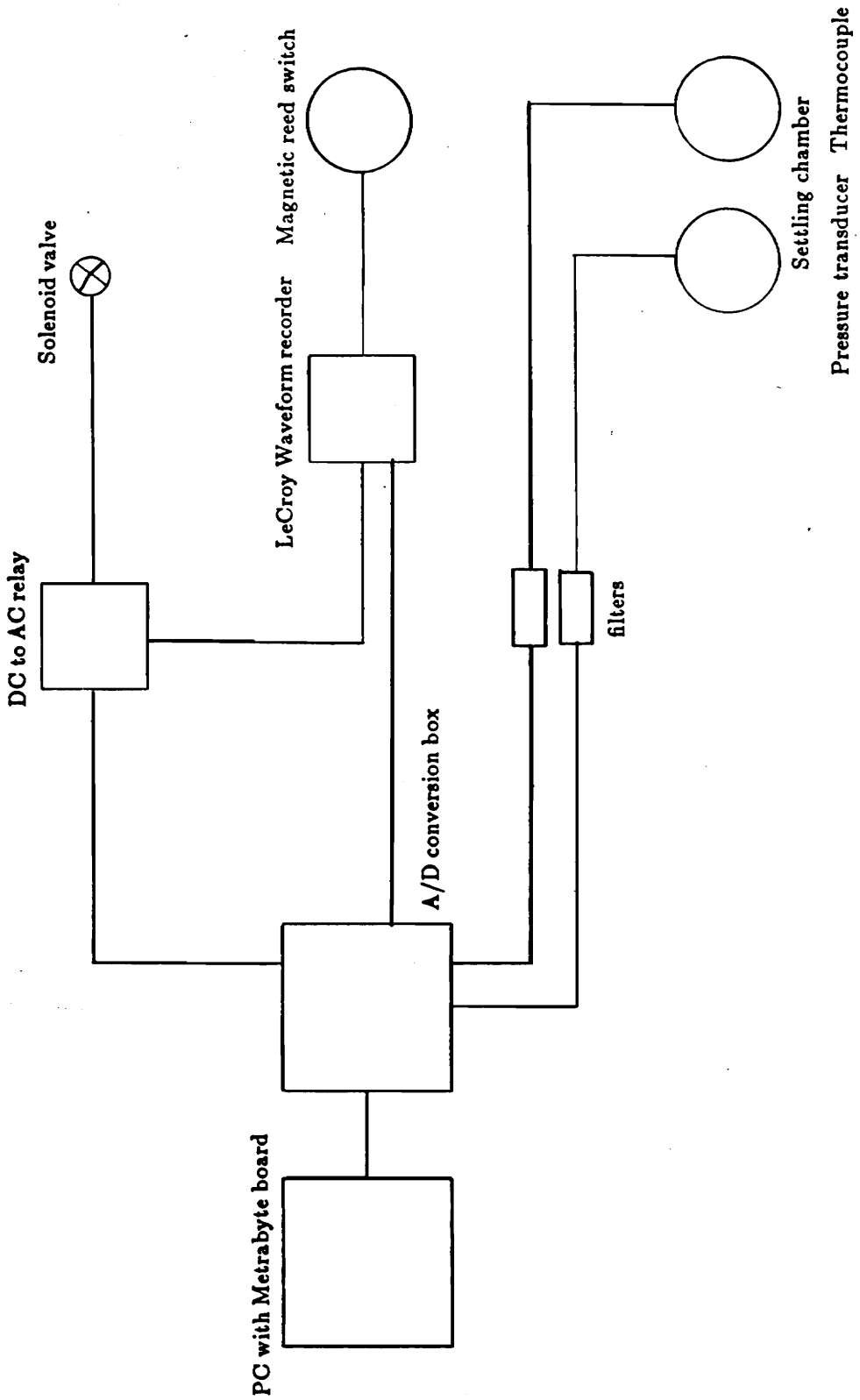


Figure 5: Schematic of the Instrumentation

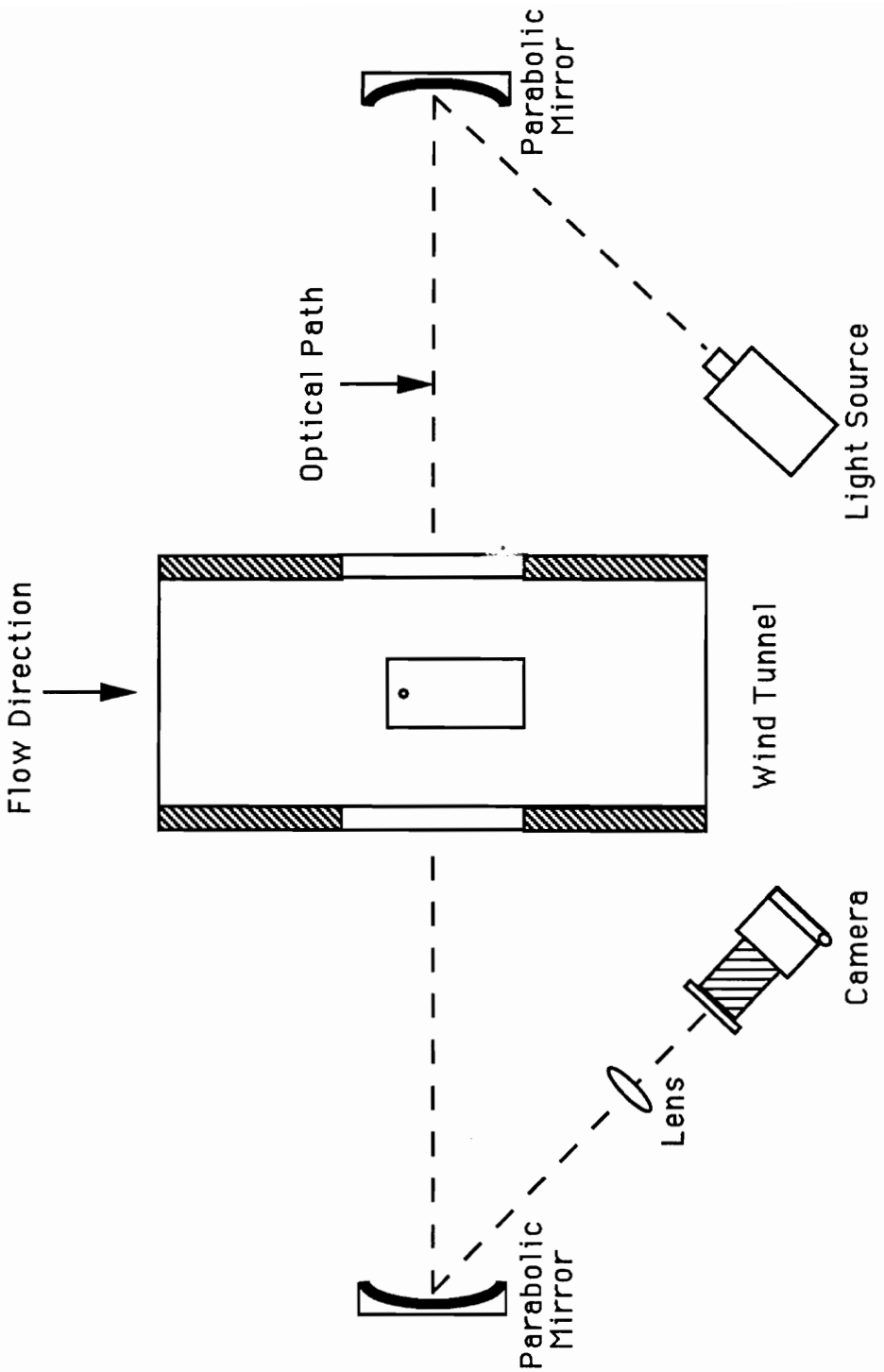


Figure 6: Sketch of the Shadowgraph Optical System

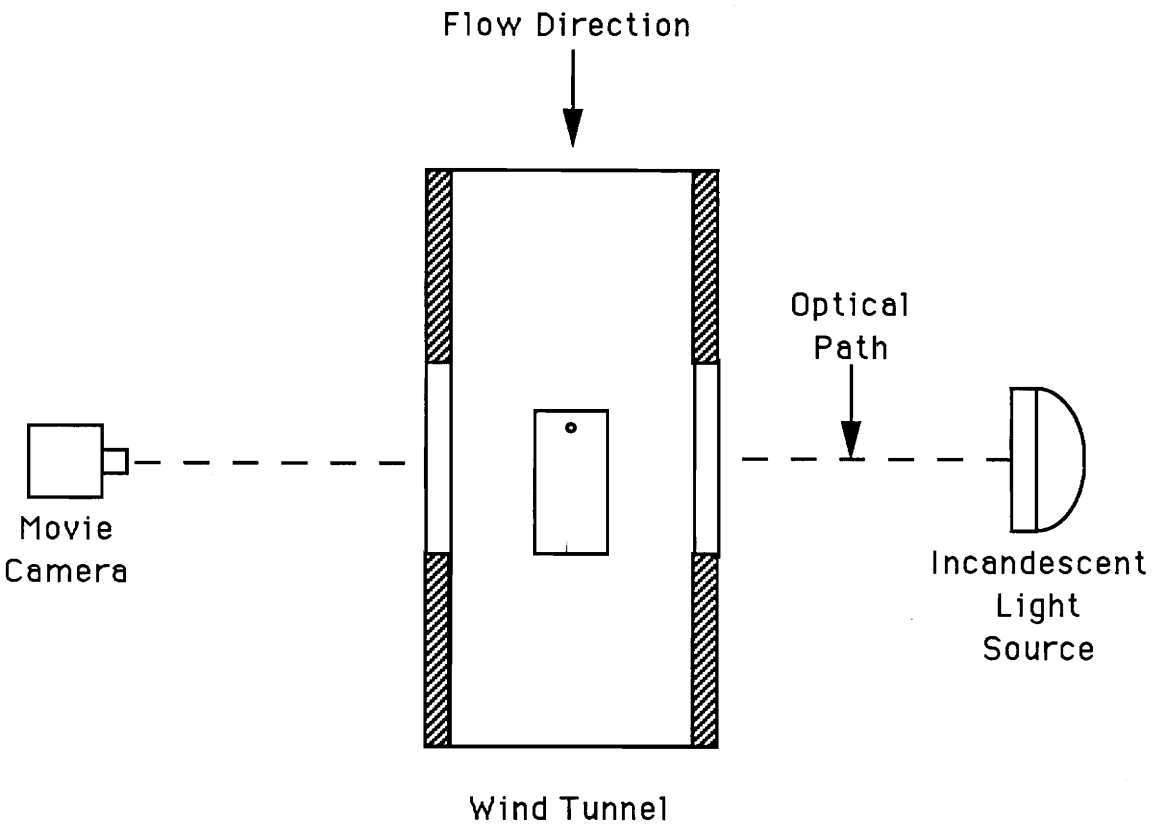


Figure 7: Sketch of the Movie Optical System

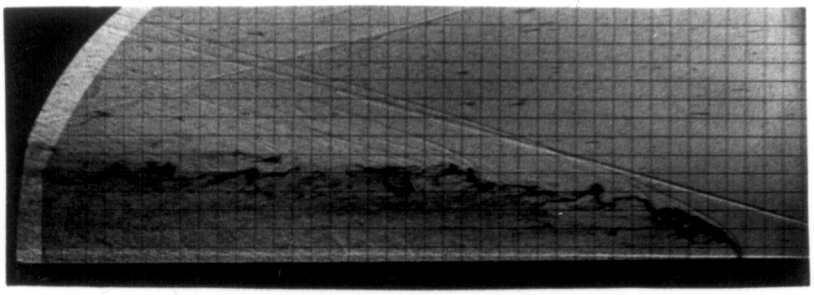

Run 246(glycerin) : $M = 4.0, \bar{q} = 7.2$
injector type : circular, $d_j = 2$ mm, $\alpha_j = 90^\circ$

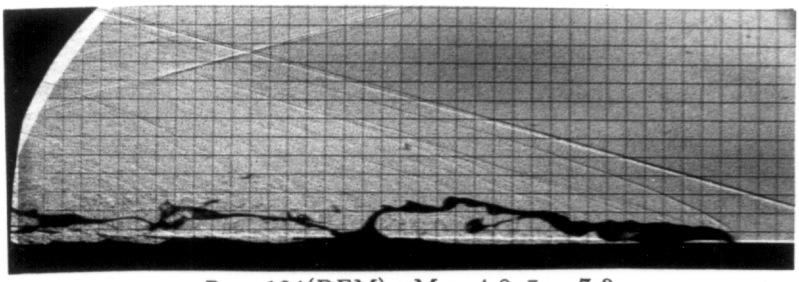

Run 164(DEM) : $M = 4.0, \bar{q} = 7.2$
injector type : circular, $d_j = 2$ mm, $\alpha_j = 90^\circ$

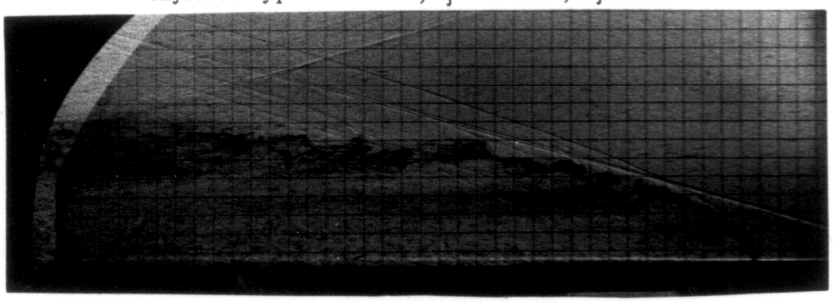

Run 243(glycerin) : $M = 4.0, \bar{q} = 10$
injector type : circular, $d_j = 2$ mm, $\alpha_j = 90^\circ$

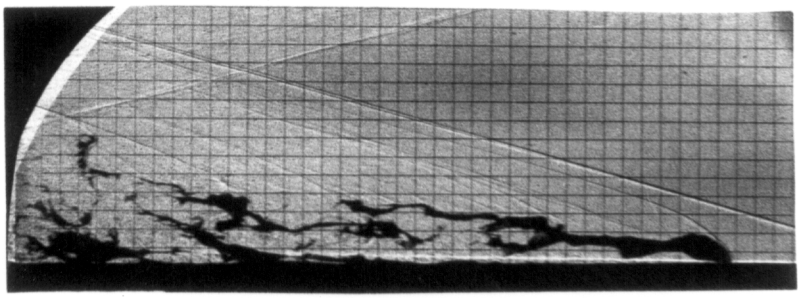

Run 163(DEM) : $M = 4.0, \bar{q} = 10$
injector type : circular, $d_j = 2$ mm, $\alpha_j = 90^\circ$

Figure 8: Non-Newtonian and Newtonian Fluid Comparison for Two Realizations

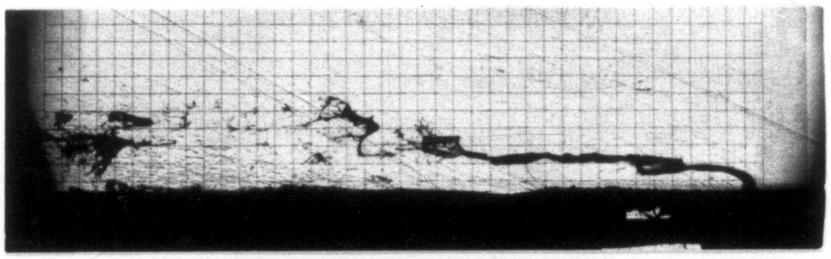

Run 124 : M = 2.4, $\bar{q}$ = 6.5
injector type : circular, $d_j$ = 2 mm, $\alpha_j$ = 90°

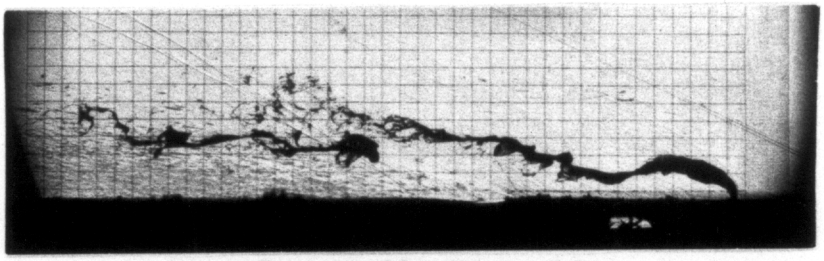

Run 121 : M = 2.4, $\bar{q}$ = 9.5
injector type : circular, $d_j$ = 2 mm, $\alpha_j$ = 90°

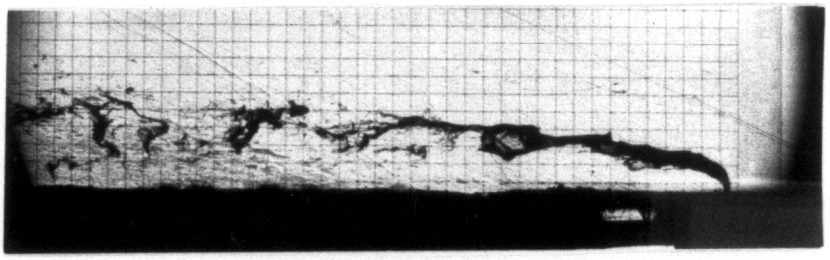

Run 118 : M = 2.4, $\bar{q}$ = 13.5
injector type : circular, $d_j$ = 2 mm, $\alpha_j$ = 90°

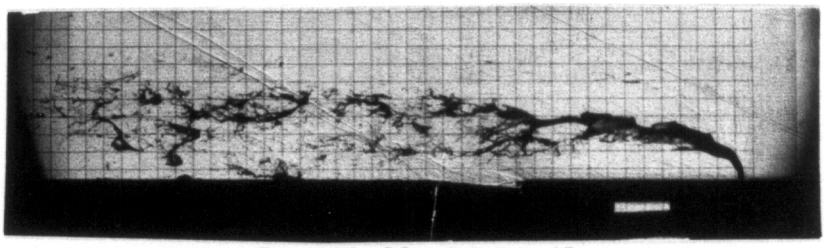

Run 109 : M = 2.4, $\bar{q}$ = 15
injector type : circular, $d_j$ = 2 mm, $\alpha_j$ = 90°

Figure 9: Effect of $\bar{q}$ on Normal Injection at Mach 2.4, First Realization

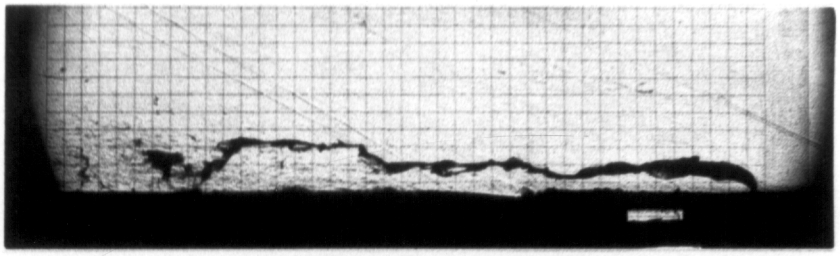

Run 125 : M = 2.4, $\bar{q}$ = 6.5
injector type : circular, $d_j$ = 2 mm, $\alpha_j$ = 90°

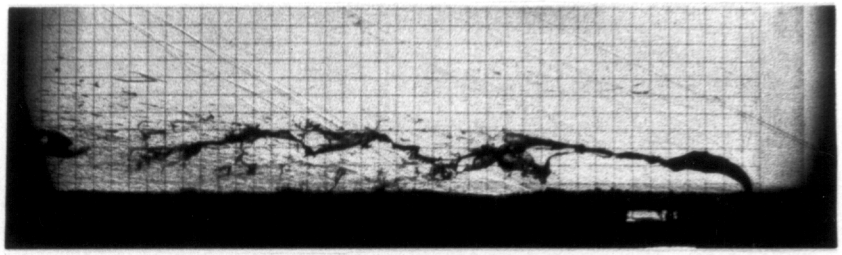

Run 122 : M = 2.4, $\bar{q}$ = 9.5
injector type : circular, $d_j$ = 2 mm, $\alpha_j$ = 90°

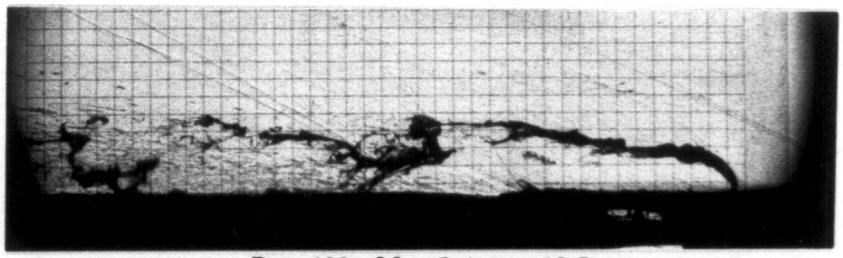

Run 120 : M = 2.4, $\bar{q}$ = 13.5
injector type : circular, $d_j$ = 2 mm, $\alpha_j$ = 90°

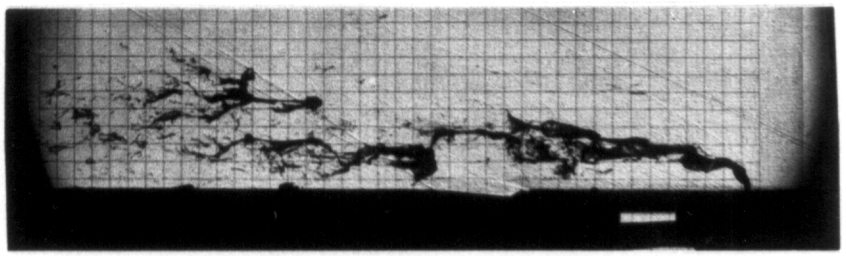

Run 110 : M = 2.4, $\bar{q}$ = 15
injector type : circular, $d_j$ = 2 mm, $\alpha_j$ = 90°

Figure 10: Effect of $\bar{q}$ on Normal Injection at Mach 2.4, Second Realization

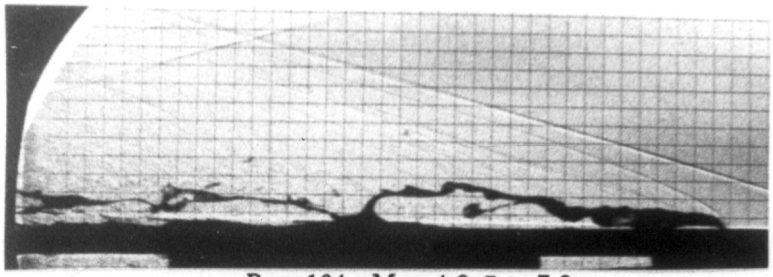

Run 164 : M = 4.0, $\bar{q}$ = 7.2
injector type : circular, $d_j$ = 2 mm, $\alpha_j$ = 90°

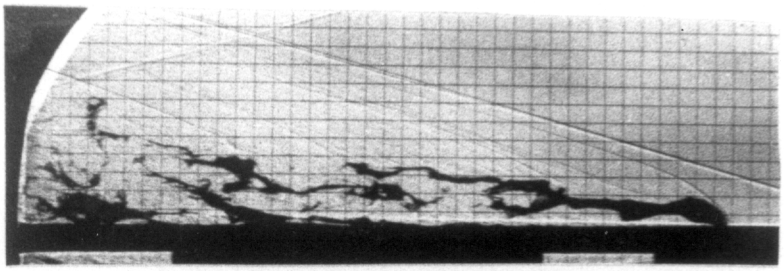

Run 163 : M = 4.0, $\bar{q}$ = 10
injector type : circular, $d_j$ = 2 mm, $\alpha_j$ = 90°

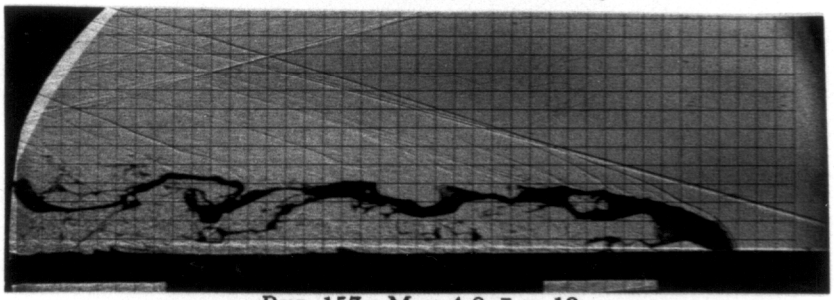

Run 157 : M = 4.0, $\bar{q}$ = 13
injector type : circular, $d_j$ = 2 mm, $\alpha_j$ = 90°

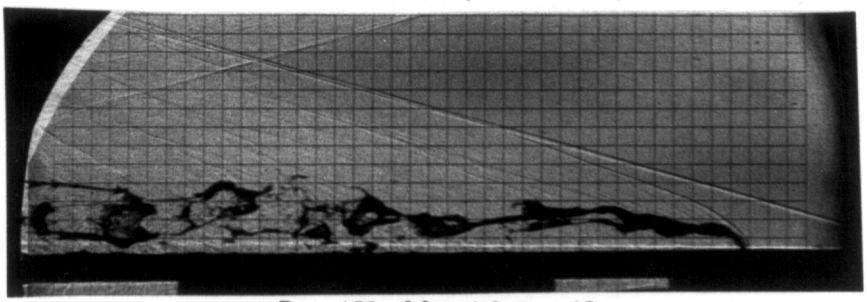

Run 159 : M = 4.0, $\bar{q}$ = 15
injector type : circular, $d_j$ = 2 mm, $\alpha_j$ = 90°

Figure 11: Effect of $\bar{q}$ on Normal Injection at Mach 4.0 (continued next page)

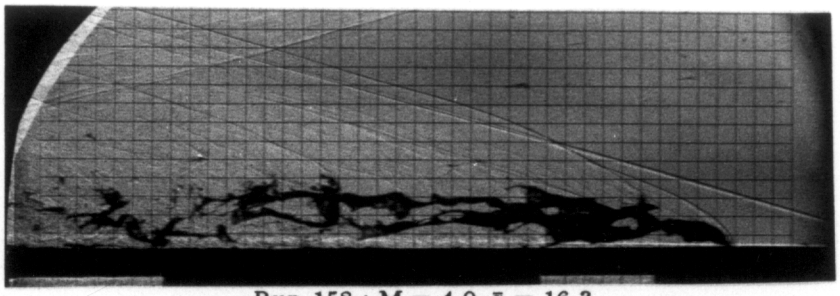

Run 158 : M = 4.0, $\bar{q}$ = 16.3
injector type : circular, $d_j$ = 2 mm, $\alpha_j$ = 90°

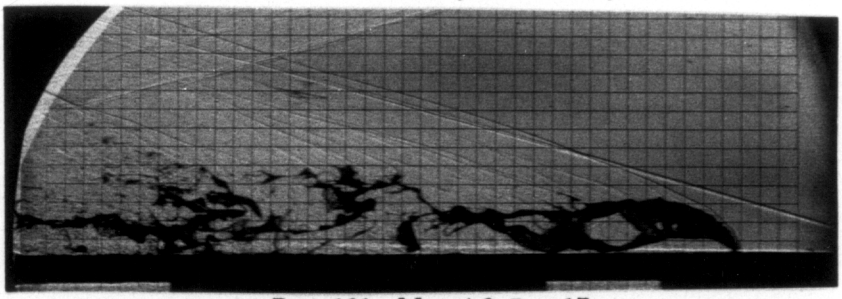

Run 161 : M = 4.0, $\bar{q}$ = 17
injector type : circular, $d_j$ = 2 mm, $\alpha_j$ = 90°

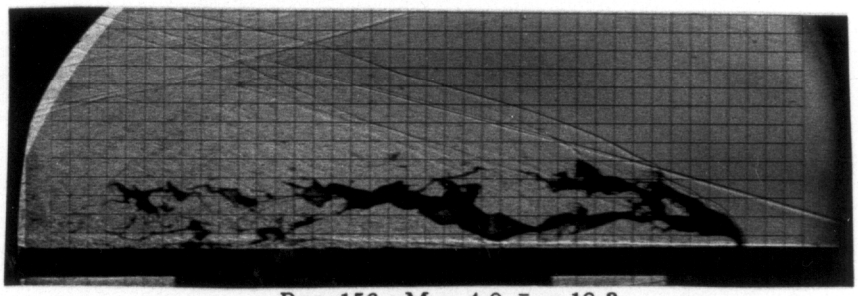

Run 156 : M = 4.0, $\bar{q}$ = 19.3
injector type : circular, $d_j$ = 2 mm, $\alpha_j$ = 90°

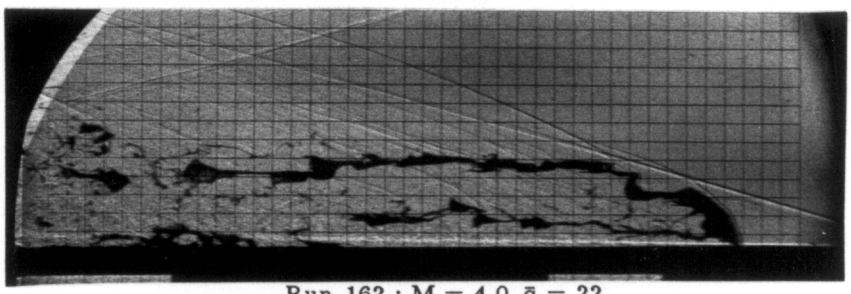

Run 162 : M = 4.0, $\bar{q}$ = 22
injector type : circular, $d_j$ = 2 mm, $\alpha_j$ = 90°

Figure 11: Effect of $\bar{q}$ on Normal Injection at Mach 4.0 (concluded)

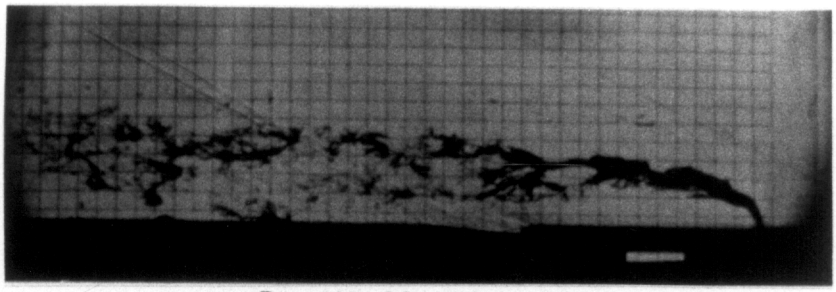

Run 109 : M = 2.4, $\bar{q}$ = 15
injector type : circular, $d_j$ = 2 mm, $\alpha_j$ = 90°

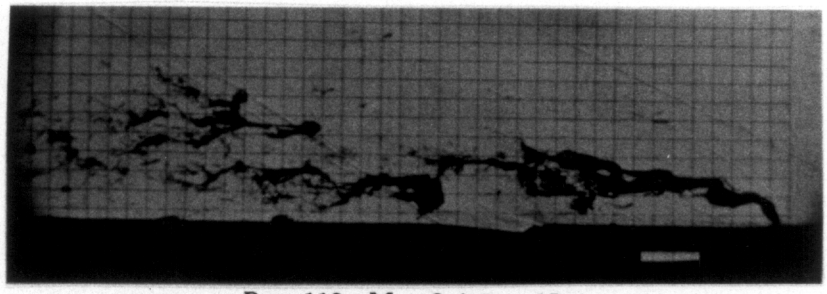

Run 110 : M = 2.4, $\bar{q}$ = 15
injector type : circular, $d_j$ = 2 mm, $\alpha_j$ = 90°

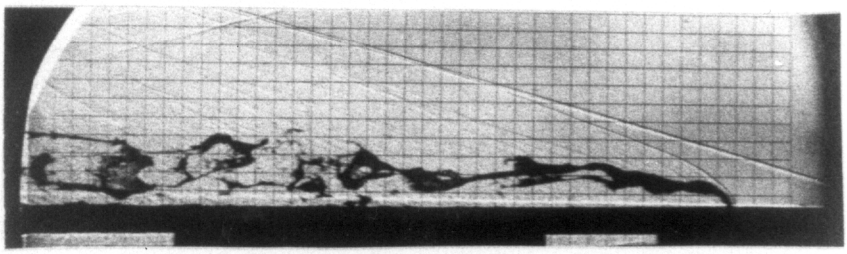

Run 159 : M = 4.0, $\bar{q}$ = 15
injector type : circular, $d_j$ = 2 mm, $\alpha_j$ = 90°

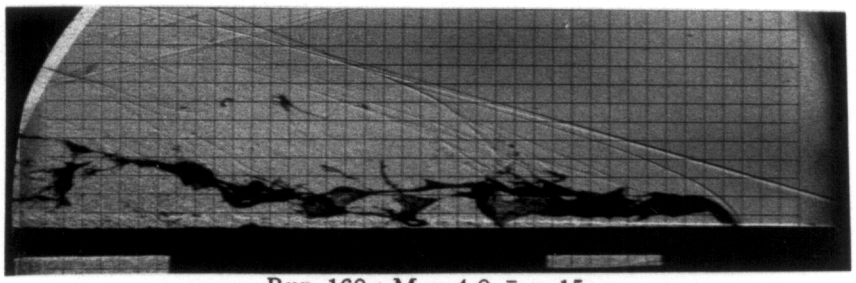

Run 160 : M = 4.0, $\bar{q}$ = 15
injector type : circular, $d_j$ = 2 mm, $\alpha_j$ = 90°

Figure 12: Effect of Mach Number for Normal Injection with constant $\bar{q}$

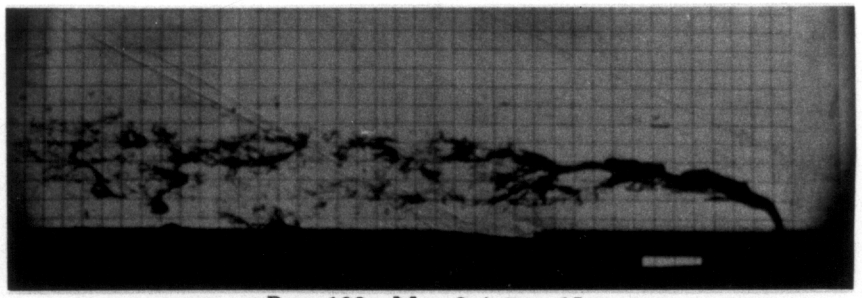

Run 109 : M = 2.4, $\bar{q}$ = 15
injector type : circular, $d_j$ = 2 mm, $\alpha_j$ = 90°

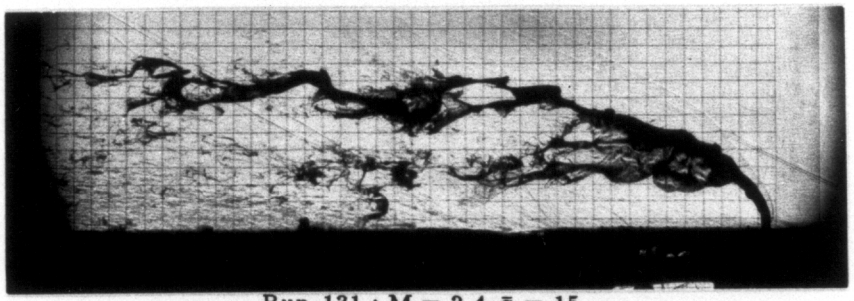

Run 131 : M = 2.4, $\bar{q}$ = 15
injector type : circular, $d_j$ = 3.25 mm, $\alpha_j$ = 90°

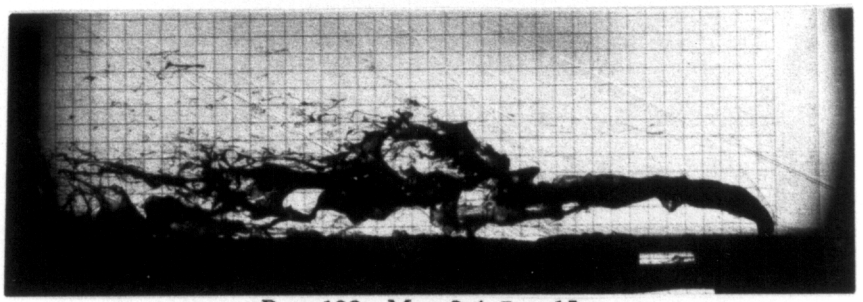

Run 128 : M = 2.4, $\bar{q}$ = 15
injector type : circular, $d_j$ = 5 mm, $\alpha_j$ = 90°

Figure 13: Effect of $d_j$ at Mach 2.4, First Realization

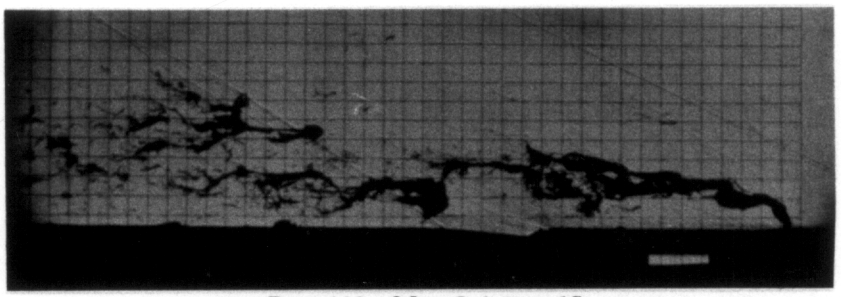

Run 110 : M = 2.4, $\bar{q}$ = 15
injector type : circular, $d_j$ = 2 mm, $\alpha_j$ = 90°

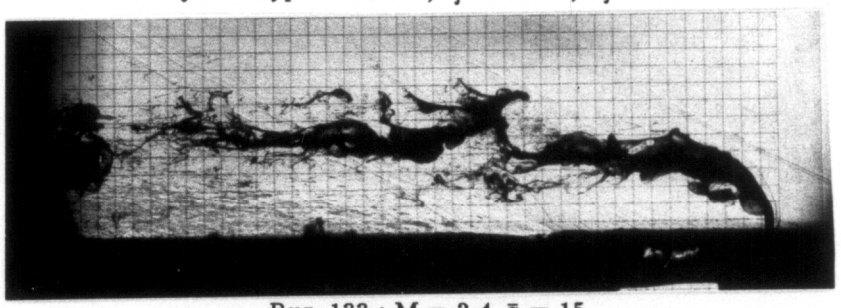

Run 133 : M = 2.4, $\bar{q}$ = 15
injector type : circular, $d_j$ = 3.25 mm, $\alpha_j$ = 90°

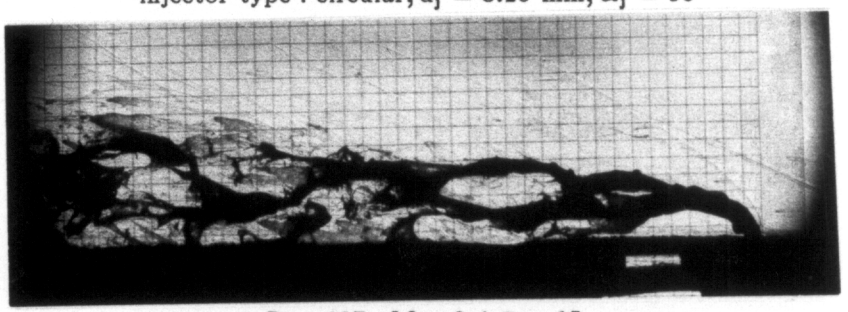

Run 127 : M = 2.4, $\bar{q}$ = 15
injector type : circular, $d_j$ = 5 mm, $\alpha_j$ = 90°

Figure 14: Effect of $d_j$ at Mach 2.4, Second Realization

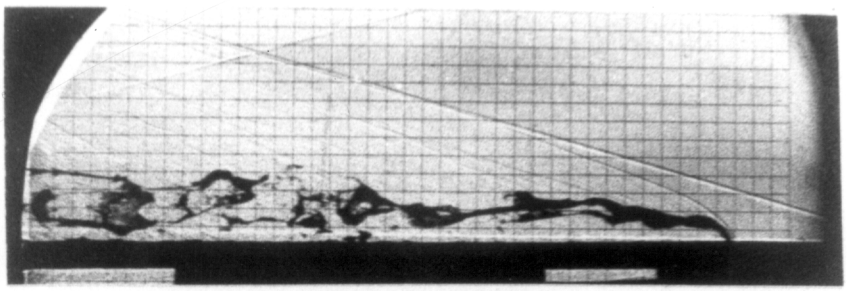

Run 159 : M = 4.0, $\bar{q}$ = 15
injector type : circular, $d_j$ = 2 mm, $\alpha_j$ = 90°

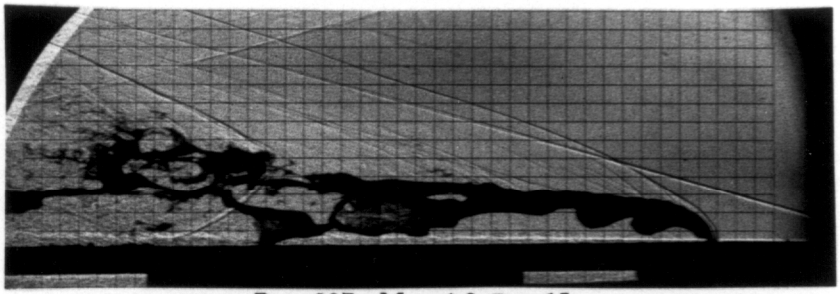

Run 207 : M = 4.0, $\bar{q}$ = 15
injector type : circular, $d_j$ = 3.25 mm, $\alpha_j$ = 90°

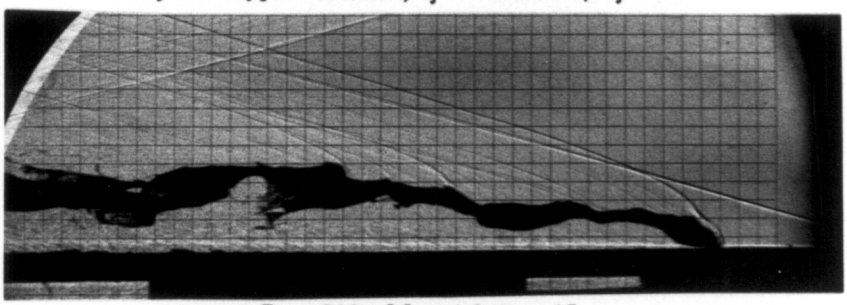

Run 210 : M = 4.0, $\bar{q}$ = 15
injector type : circular, $d_j$ = 5 mm, $\alpha_j$ = 90°

Figure 15: Effect of $d_j$ at Mach 4.0

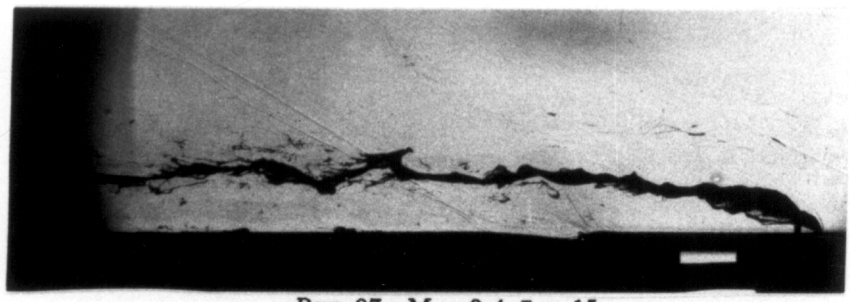

Run 97 : M = 2.4, $\bar{q}$ = 15
injector type : twincircular, $d_j$ = 2 mm, $\alpha_j$ = 90°

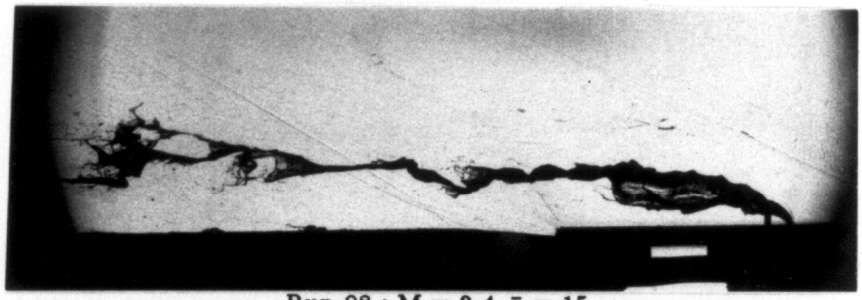

Run 98 : M = 2.4, $\bar{q}$ = 15
injector type : twincircular, $d_j$ = 2 mm, $\alpha_j$ = 90°

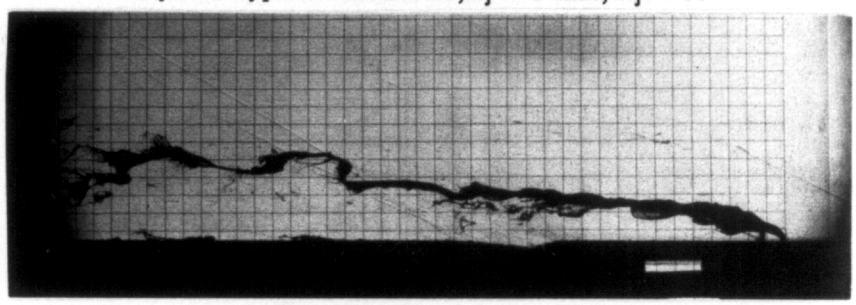

Run 99 : M = 2.4, $\bar{q}$ = 15
injector type : twincircular, $d_j$ = 2 mm, $\alpha_j$ = 90°

Figure 16: Effect of Twin In-line Jets at Mach 2.4 with $\bar{q} = 15$.

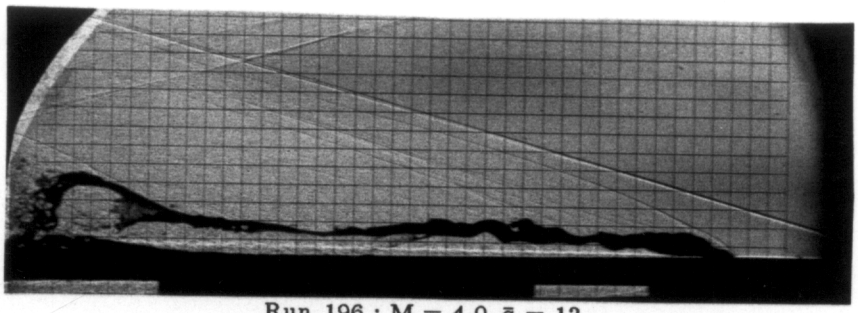

Run 196 : M = 4.0, $\bar{q}$ = 12
injector type : twincircular, $d_j$ = 2 mm, $\alpha_j$ = 90°

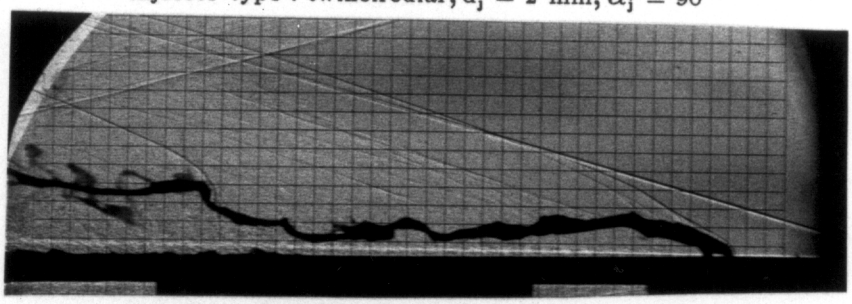

Run 200 : M = 4.0, $\bar{q}$ = 15
injector type : twincircular, $d_j$ = 2 mm, $\alpha_j$ = 90°

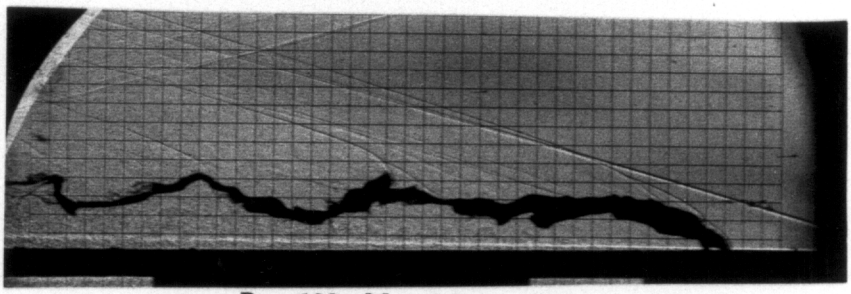

Run 198 : M = 4.0, $\bar{q}$ = 19.3
injector type : twincircular, $d_j$ = 2 mm, $\alpha_j$ = 90°

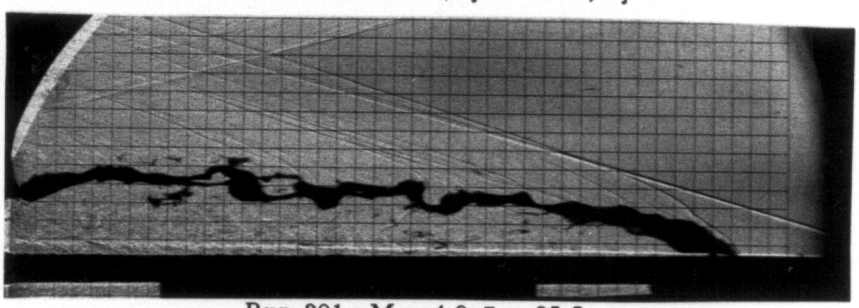

Run 201 : M = 4.0, $\bar{q}$ = 25.5
injector type : twincircular, $d_j$ = 2 mm, $\alpha_j$ = 90°

Figure 17: Effect of $\bar{q}$ on Twin In-line Jets at Mach 4.0

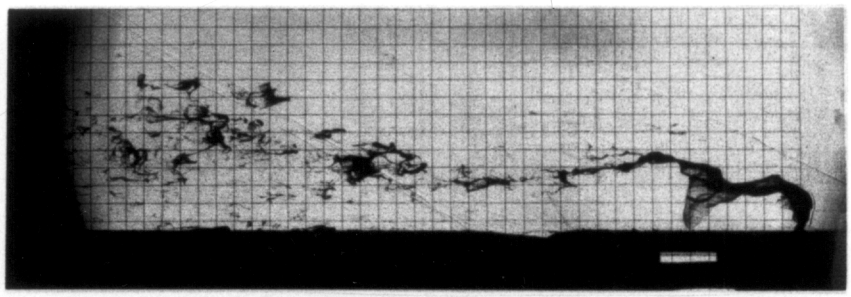

Run 101 : M = 2.4, $\bar{q}$ = 15
injector type : circular, $d_j$ = 2 mm, $\alpha_j$ = 45°

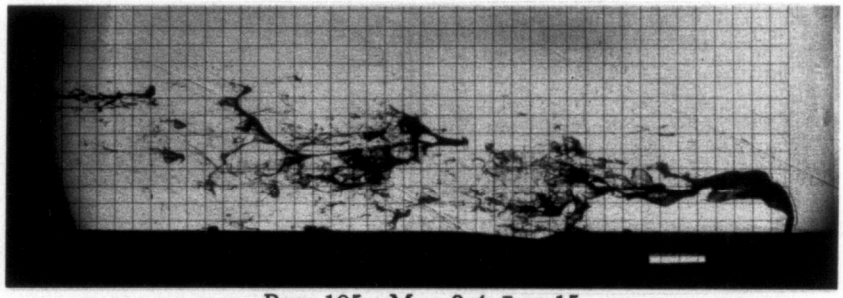

Run 105 : M = 2.4, $\bar{q}$ = 15
injector type : circular, $d_j$ = 2 mm, $\alpha_j$ = 60°

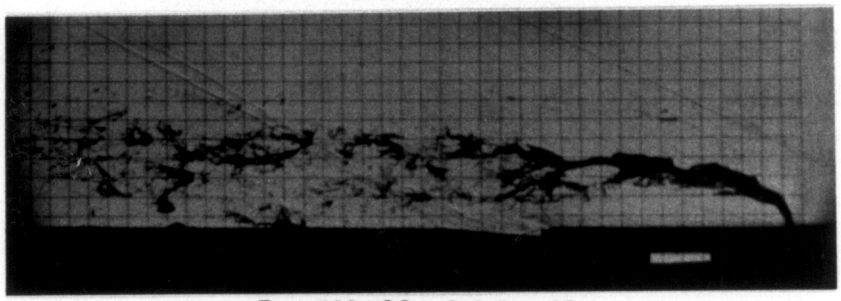

Run 109 : M = 2.4, $\bar{q}$ = 15
injector type : circular, $d_j$ = 2 mm, $\alpha_j$ = 90°

Figure 18: Effect of Upstream Injection at Mach 2.4

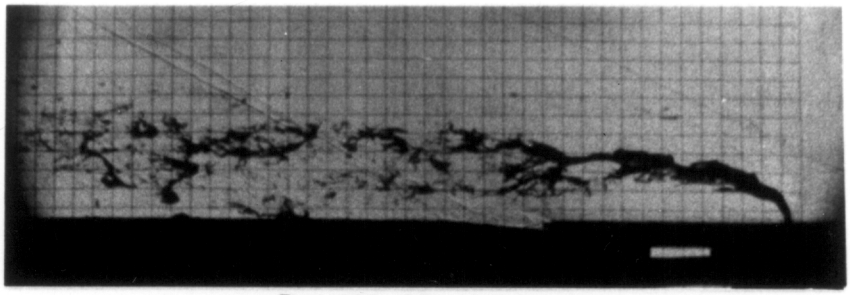

Run 109 : M = 2.4, $\bar{q}$ = 15
injector type : circular, $d_j$ = 2 mm, $\alpha_j$ = 90°

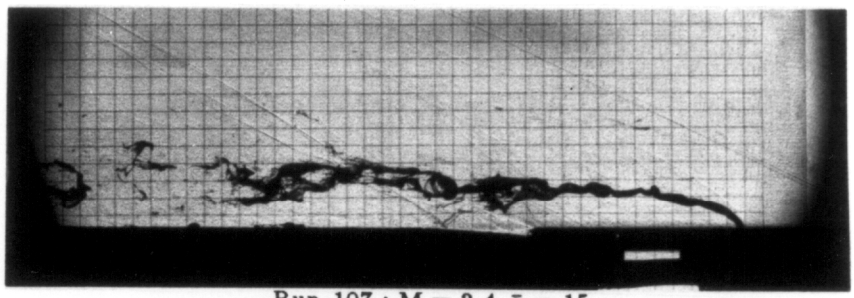

Run 107 : M = 2.4, $\bar{q}$ = 15
injector type : circular, $d_j$ = 2 mm, $\alpha_j$ = 120°

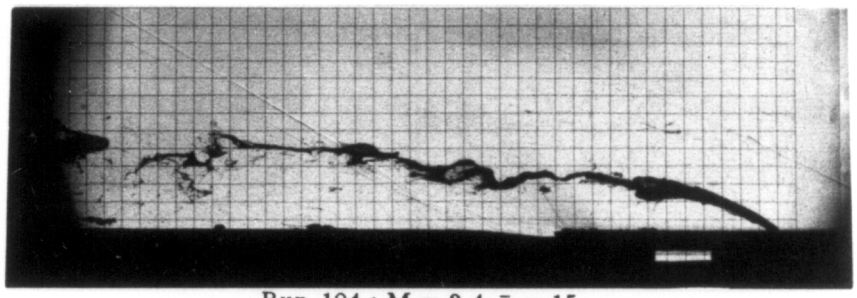

Run 104 : M = 2.4, $\bar{q}$ = 15
injector type : circular, $d_j$ = 2 mm, $\alpha_j$ = 135°

Figure 19: Effect of Downstream Injection at Mach 2.4

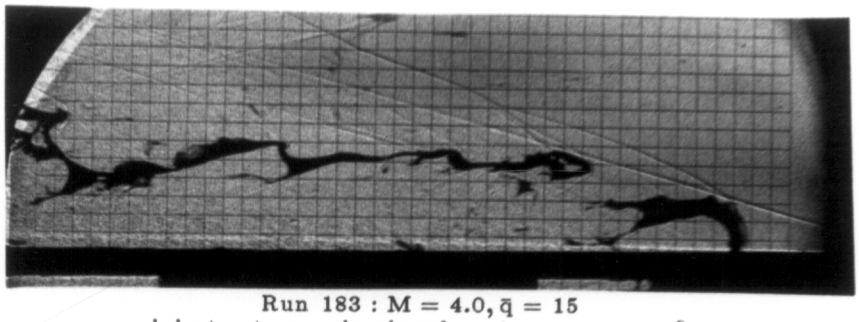

Run 183 : M = 4.0, $\bar{q}$ = 15
injector type : circular, $d_j$ = 2 mm, $\alpha_j$ = 45°

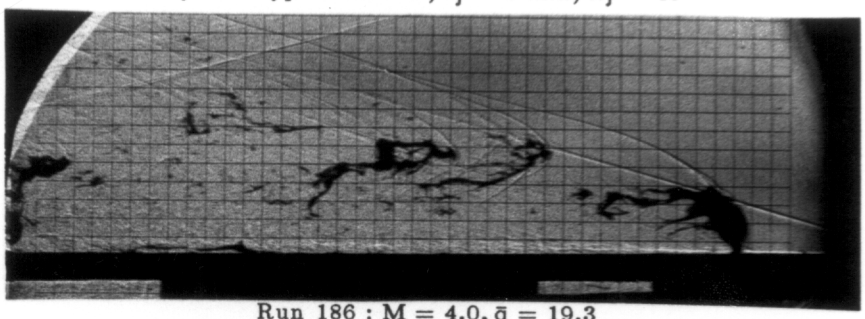

Run 186 : M = 4.0, $\bar{q}$ = 19.3
injector type : circular, $d_j$ = 2 mm, $\alpha_j$ = 45°

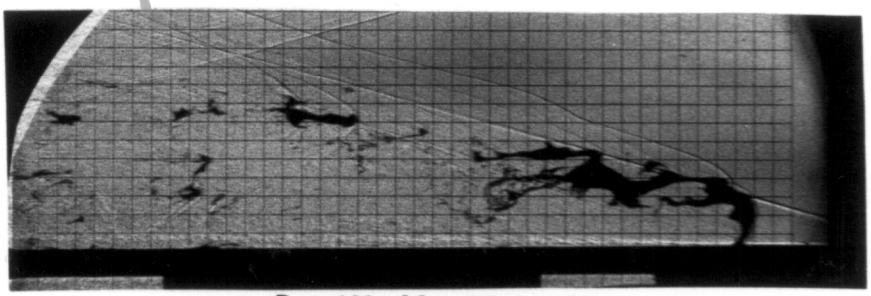

Run 189 : M = 4.0, $\bar{q}$ = 22
injector type : circular, $d_j$ = 2 mm, $\alpha_j$ = 45°

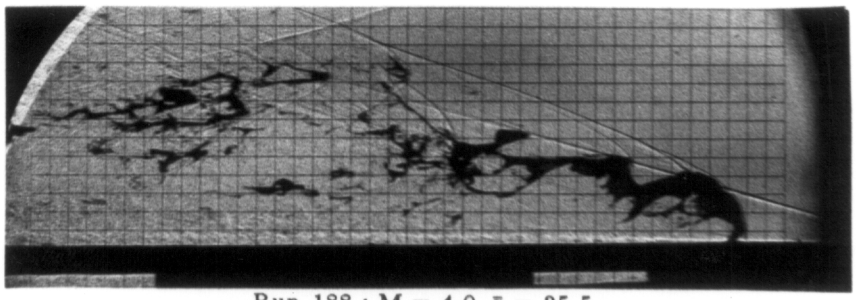

Run 188 : M = 4.0, $\bar{q}$ = 25.5
injector type : circular, $d_j$ = 2 mm, $\alpha_j$ = 45°

Figure 20: Effect of $\bar{q}$ on Upstream Injection at Mach 4.0, $\alpha_j = 45^\circ$

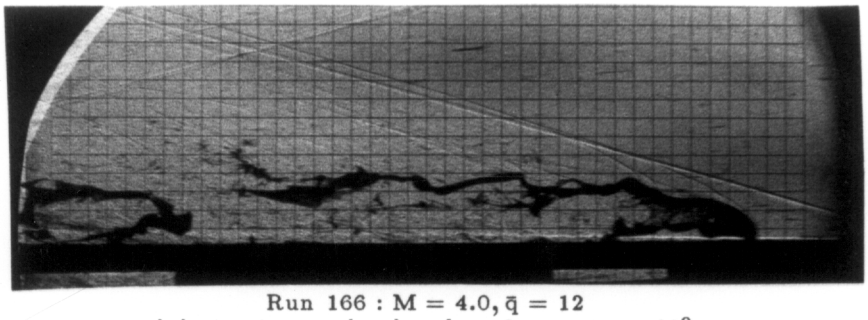

Run 166 : M = 4.0, $\bar{q}$ = 12
injector type : circular, $d_j$ = 2 mm, $\alpha_j$ = 60°

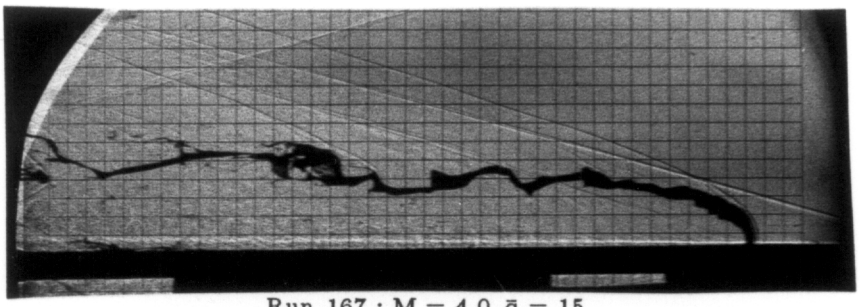

Run 167 : M = 4.0, $\bar{q}$ = 15
injector type : circular, $d_j$ = 2 mm, $\alpha_j$ = 60°

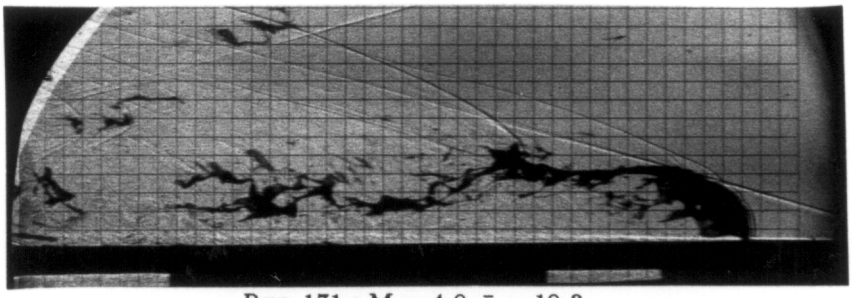

Run 171 : M = 4.0, $\bar{q}$ = 19.3
injector type : circular, $d_j$ = 2 mm, $\alpha_j$ = 60°

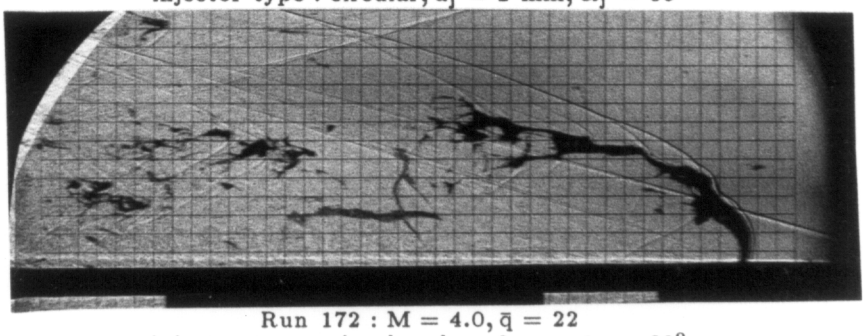

Run 172 : M = 4.0, $\bar{q}$ = 22
injector type : circular, $d_j$ = 2 mm, $\alpha_j$ = 60°

Figure 21: Effect of $\bar{q}$ on Upstream Injection at Mach 4.0, $\alpha_j = 60^o$

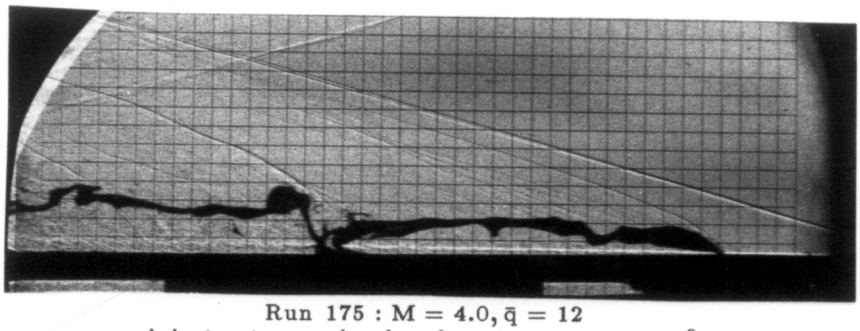

Run 175 : M = 4.0, $\bar{q}$ = 12
injector type : circular, $d_j$ = 2 mm, $\alpha_j$ = 120°

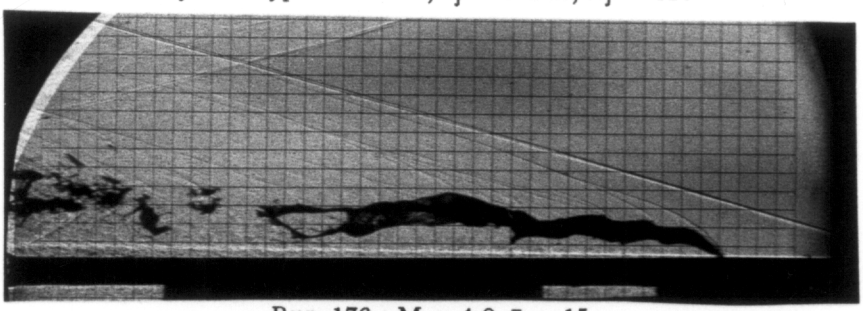

Run 176 : M = 4.0, $\bar{q}$ = 15
injector type : circular, $d_j$ = 2 mm, $\alpha_j$ = 120°

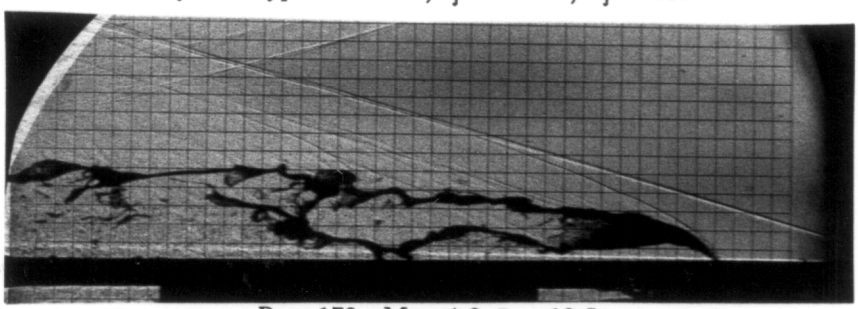

Run 178 : M = 4.0, $\bar{q}$ = 18.5
injector type : circular, $d_j$ = 2 mm, $\alpha_j$ = 120°

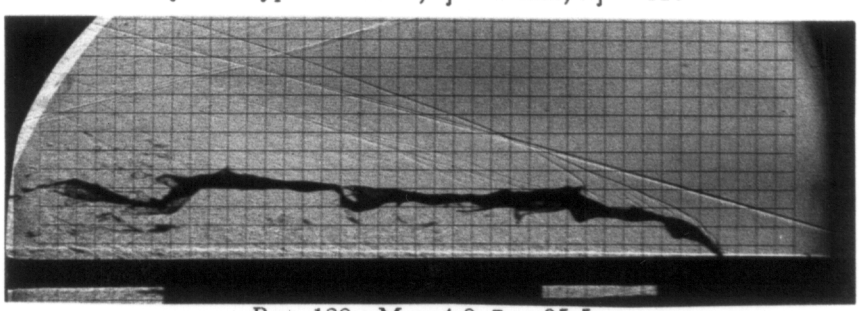

Run 180 : M = 4.0, $\bar{q}$ = 25.5
injector type : circular, $d_j$ = 2 mm, $\alpha_j$ = 120°

Figure 22: Effect of $\bar{q}$ on Downstream Injection at Mach 4.0, $\alpha_j = 120^o$

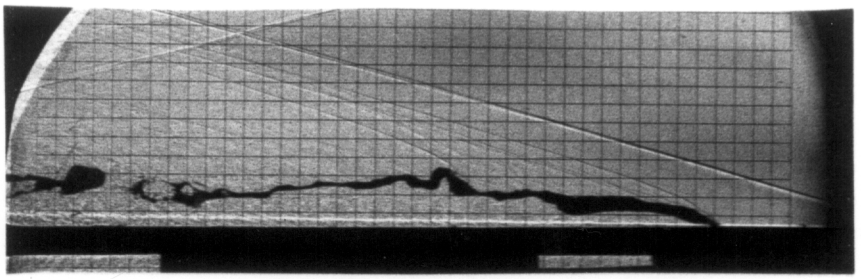

Run 191 : M = 4.0, $\bar{q}$ = 12
injector type : circular, $d_j$ = 2 mm, $\alpha_j$ = 135°

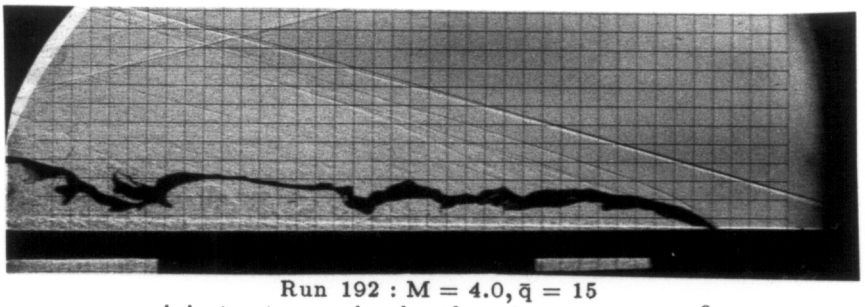

Run 192 : M = 4.0, $\bar{q}$ = 15
injector type : circular, $d_j$ = 2 mm, $\alpha_j$ = 135°

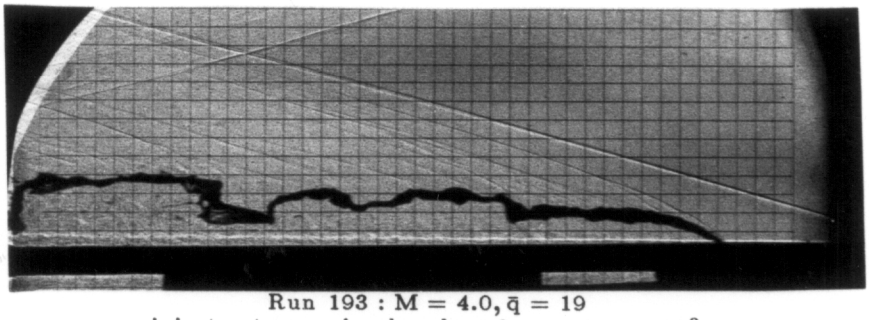

Run 193 : M = 4.0, $\bar{q}$ = 19
injector type : circular, $d_j$ = 2 mm, $\alpha_j$ = 135°

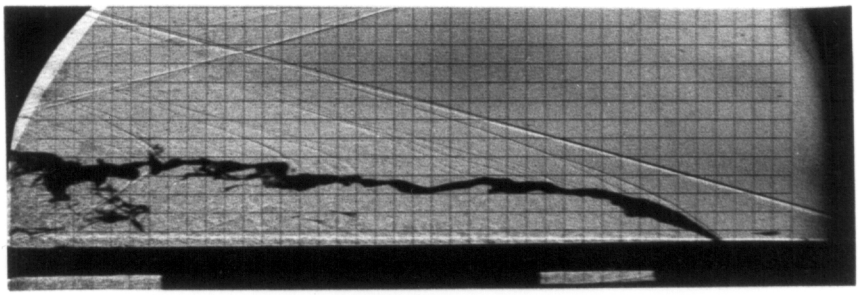

Run 194 : M = 4.0, $\bar{q}$ = 25.5
injector type : circular, $d_j$ = 2 mm, $\alpha_j$ = 135°

Figure 23: Effect of $\bar{q}$ on Downstream Injection at Mach 4.0, $\alpha_j = 135°$

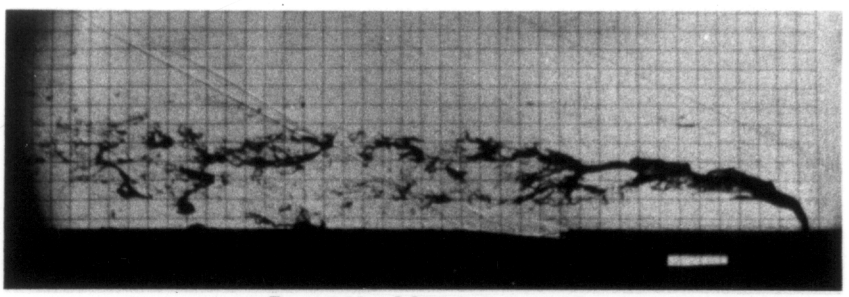

Run 109 : M = 2.4, $\bar{q}$ = 15
injector type : circular, $d_j$ = 2 mm, $\alpha_j$ = 90°

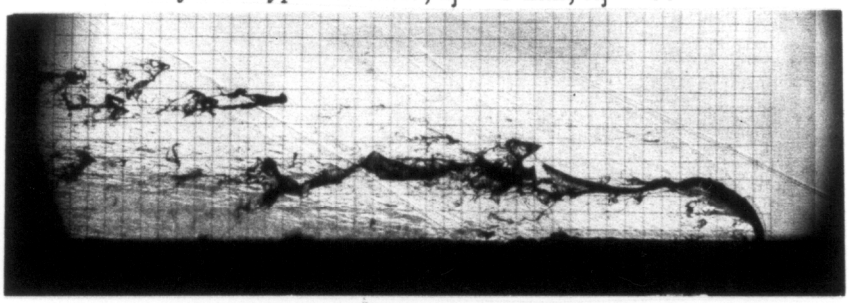

Run 139 : M = 2.4, $\bar{q}$ = 15
injector type : rectangular — aligned, $d_j$ = 2 mm, $\alpha_j$ = 90°

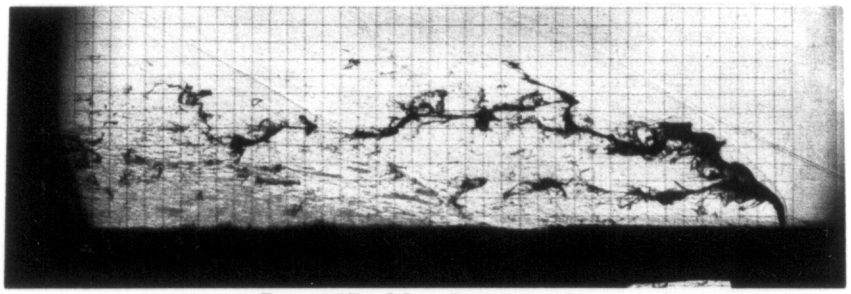

Run 137 : M = 2.4, $\bar{q}$ = 15
injector type : rectangular — across, $d_j$ = 2 mm, $\alpha_j$ = 90°

Figure 24: Effect of Rectangular Shape at Mach 2.4

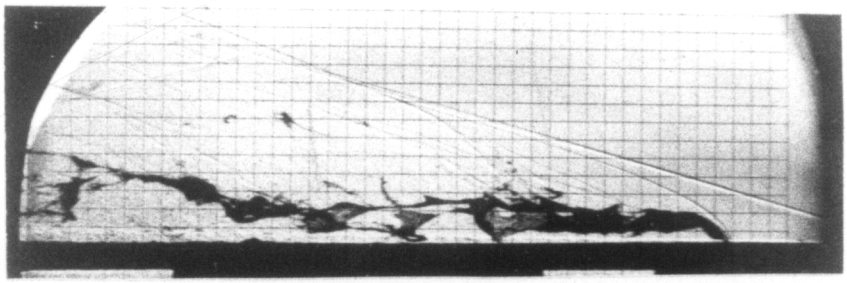

Run 160 : $M = 4.0, \bar{q} = 15$
injector type : circular, $d_j = 2$ mm, $\alpha_j = 90^\circ$

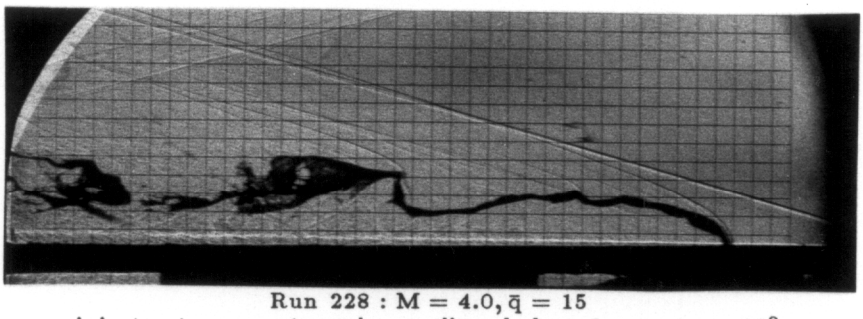

Run 228 : $M = 4.0, \bar{q} = 15$
injector type : rectangular — aligned, $d_j = 2$ mm, $\alpha_j = 90^\circ$

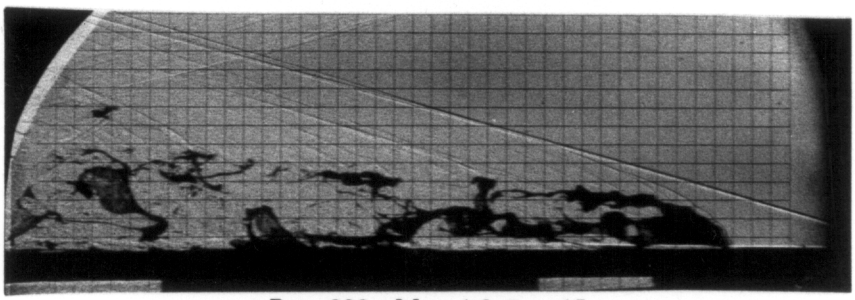

Run 220 : $M = 4.0, \bar{q} = 15$
injector type : rectangular — across, $d_j = 2$ mm, $\alpha_j = 90^\circ$

Figure 25: Effect of Rectangular Shape at Mach 4.0

(a) $\bar{q} = 5.5$

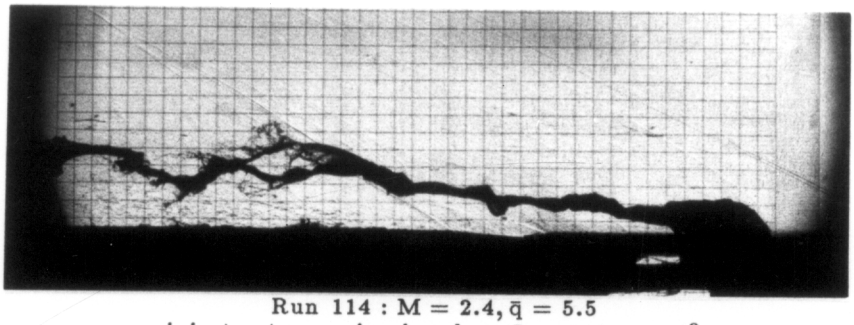

Run 114 : M = 2.4, $\bar{q}$ = 5.5
injector type : circular, $d_j$ = 5 mm, $\alpha_j = 90°$

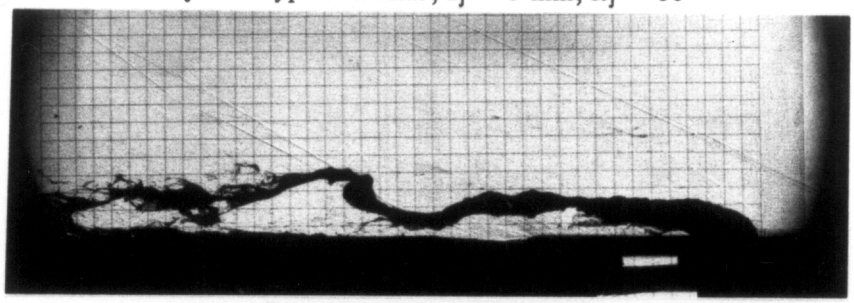

Run 116 : M = 2.4, $\bar{q}$ = 5.5
injector type : roughened circular, $d_j$ = 5 mm, $\alpha_j = 90°$

(b) $\bar{q} = 15$

Run 127 : M = 2.4, $\bar{q}$ = 15
injector type : circular, $d_j$ = 5 mm, $\alpha_j = 90°$

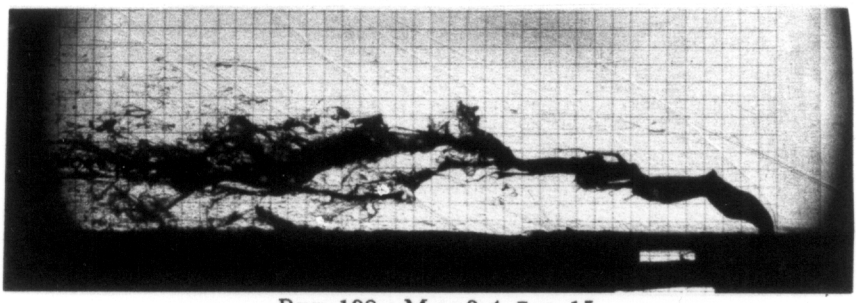

Run 129 : M = 2.4, $\bar{q}$ = 15
injector type : roughened circular, $d_j$ = 5 mm, $\alpha_j = 90°$

Figure 26: Effect of Roughness at Mach 2.4

(a) $\bar{q} = 12$

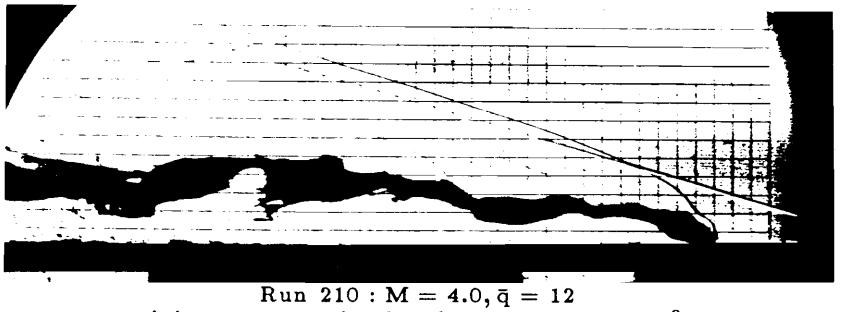

Run 210 : M = 4.0, $\bar{q}$ = 12
injector type : circular, $d_j$ = 5 mm, $\alpha_j$ = 90°

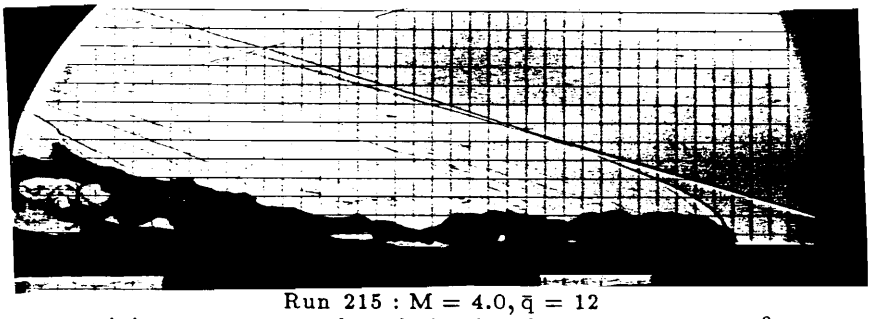

Run 215 : M = 4.0, $\bar{q}$ = 12
injector type : roughened circular, $d_j$ = 5 mm, $\alpha_j$ = 90°

(b) $\bar{q} = 15$

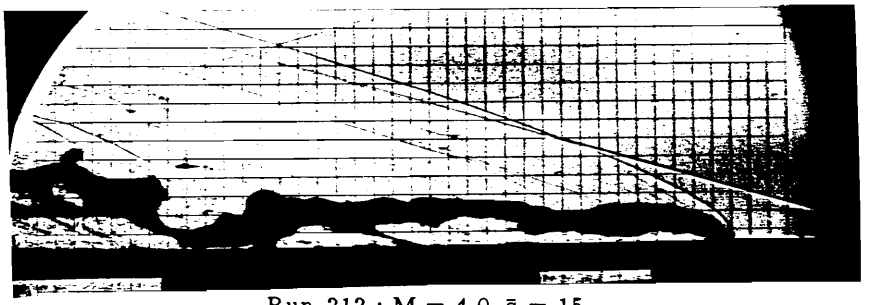

Run 212 : M = 4.0, $\bar{q}$ = 15
injector type : circular, $d_j$ = 5 mm, $\alpha_j$ = 90°

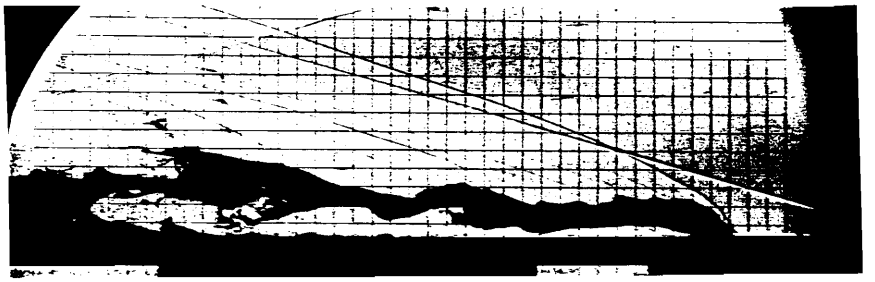

Run 216 : M = 4.0, $\bar{q}$ = 15
injector type : roughened circular, $d_j$ = 5 mm, $\alpha_j$ = 90°

Figure 27: Effect of Roughness at Mach 4.0


Figure 28: High Speed Movie at Mach 2.4, $d_j = 2.0$ mm, $\bar{q} = 20$

# APPENDIX : Computer Programs

Listing of INJECT.BAS

```
'*****************************************************************
'
CLEAR, 59000! 'reduce workspace to 48K
SCREEN 0,0,0 : CLS : KEY OFF : WIDTH 80
DIM A$(30),B$(30),TU$(30),TD$(30),TRAV(1000)
FALSE=0:TRUE=NOT FALSE:XOFF$=CHR$(19):XON$=CHR$(17)
CLOSE
PAUSE=FALSE
PRINT "Hit any key when ready . . . ":PRINT
A$=INKEY$ : IF A$="" THEN 210
'
PRINT"-Data will be dumped under B:RAWDAT , B:PRES
PRINT
TU$="V39 D342 Z0 R1 V350 D342 Z1 R1"
'
'————————— STEP 1 ————————————————————
DEF SEG = 0 'find BASIC's segment
SG = 256 * PEEK(H511) + PEEK(H510)
SG = SG + 49152!/16
DEF SEG = SG 'SG = load location
BLOAD "DASH16.BIN", 0 'for DASH16.BIN
'
```

```
'————————— STEP 2 ————————————————————
DIM DIO%(4) 'declare data array
DIO%(0) = H300 'base I/O address
DIO%(1) = 2 'interrupt level
DIO%(2) = 3 'D.M.A. level
'Be sure that base address and DMA level correspond to switch settings
'on DASH-16!
MD% = 0 'initialize mode
FLAG% = 0 'declare error variable
DASH16 = 0 'CALL offset = 0
CALL DASH16 (MD%, DIO%(0),FLAG%) 'initialize
IF FLAG% not equal to 0 THEN PRINT"Initialization error # ";FLAG% : STOP
'
'
' Make sure that on/off valve is closed
MD% = 13
DIO%(0) = 0
CALL DASH16 (MD%, DIO%(0), FLAG%):PRINT:PRINT "Tunnel valve closed":PRINT
IF FLAG% not equal to 0 THEN PRINT "Error # ";FLAG%;" on digital output"
'
'————————— STEP 3 ————————————————————
'Set programmable timer to output desired sample rate
INPUT "Enter tunnel pressure";MAXPSI
VOLT=MAXPSI/94
```

```
 DATOUT%=INT(VOLT/.00296)
 '
 PRINT"SAMPLE RATE = 1,000,000 / (N1 * N2)"
INPUT "Enter N1 and N2 :",F1%,F2%
SR%=1000000!/F1%/F2% :PRINT"Sampling Rate per channel = "SR%" Hz"
INPUT"Is sampling rate correct ¡y/n¿ ?:",B$
IF B$="y" OR B$="Y" THEN 740 ELSE 700
PRINT
DIO%(0) = F1%
DIO%(1) = F2%
MD% = 17 'timer set mode
CALL DASH16 (MD%, DIO%(0),FLAG%)
IF FLAG% not equal to 0 THEN PRINT "Error in setting timer. Error # ";FLAG%:STOP
'
'————————— STEP 4 ————————————————————
'If you skip this step, scan limits will default to:-
' 0 to 7 for 8 channel differential input configuration
' 0 to 15 for 16 channel single ended input configuration
'Now find out what you want for scan limits:-
INPUT "Lower channel scan limit (0-7 diff., 0-15 s.e.)? : ",LL%
INPUT "Upper channel scan limit (0-7 diff., 0-15 s.e.)? : ",UL%
'Set the limits using mode 1
DIO%(0) = LL% 'lower limit
DIO%(1) = UL% 'upper limit
```

```
MD% = 1
CALL DASH16 (MD%, DIO%(0),FLAG%)
IF FLAG% not equal to 0 THEN PRINT"Error in setting scan limits # ";FLAG% : STOP
PRINT
'
'————————— STEP 5 ————————————————————
'Set conversions, delay parameters, PSI system
INPUT "Enter total number of A/D conversions :",N% : PRINT
INPUT "Enter time delay (sec) before starting tunnel";SEC
 LIM3=SEC*320
 INPUT "enter time delay from valve open to injection";SEC
 LIM = SEC * 320
 INPUT"Enter time (sec) for data collection";SEC
 LIM2 = SEC * 320
'————————————————————————————————————————
'
 PRINT:PRINT"Hit any key to begin..." 'start tunnel and take data
 IF INKEY$="" THEN 1090
 FOR ZZ=1 TO LIM3:NEXT ZZ 'delay tunnel start
'
'————————————STEP 6 ————————————————————
'
' Set control valve circuit for proper operating pressure
 MD%=15
```

```
DIO%(0) = 1
DIO%(1) = DATOUT%
CALL DASH16 (MD%, DIO%(0), FLAG%)
IF FLAG% not equal to 0 THEN PRINT "Error # ";FLAG%;" on digital output"
'
' Write digital output using mode 13
MD% = 13
DIO%(0) = 1
CALL DASH16 (MD%, DIO%(0), FLAG%):PRINT:PRINT "Tunnel valve open":PRINT
IF FLAG% not equal to 0 THEN PRINT "Error # ";FLAG%;" on digital output"
FOR ZZ = 1 TO LIM: NEXT ZZ 'delays traverse to allow tunnel valve
'to open before moving
'DIO%(0) = 3
'CALL DASH16 (MD%, DIO%(0), FLAG%)
'IF FLAG% not equal to 0 THEN PRINT "Error # ";FLAG%;" on digital output"
'
'
'
PRINT:PRINT "A/D block scan reading . . ."
DIO%(0) = N% 'Total number of conversions
DIO%(1) = H3000 'Memory segment to dump data - hope its clear
' at 192K. Change this to suit your system.
DIO%(2) = 1 '1 = trigger from timer
DIO%(3) = 0 '0 = One shot and finish  MD%=20 'mode 20 - block scan on interrupt
```

Listing of QBAR.BAS

```
OPEN "b:rawdat" FOR INPUT AS #1
 SUM=0
 FOR N=1 TO 300
 INPUT #1 , DIGITAL
 IF DIGITAL ¡ 50 GOTO 70
 SUM=SUM+1
 ,
 NEXT N
 DT=SUM *.01
 PRINT "time for this run =";DT
 QBAR= 3.9172/(DT*DT)
 PRINT "qbar for this run =";QBAR
 END
```

# VITA

The author was born in Malden, Massachusetts on October 5, 1961. He was raised and received his elementary education in neighboring New Hampshire. He entered the Mechanical Engineering program at Northeastern University of Boston, Massachusetts in 1982 and received his Bachelor of Science degree in 1987. In the fall of 1987 the author entered the graduate program in Aerospace Engineering at Virginia Tech and as of the completion of this work is continuing his studies there.